Are Creep Events Big? Estimating Along Strike Lengths

Daniel B. Gittins[1], **Jessica C. Hawthorne**[1]

[1]Department of Earth Sciences, University of Oxford, Oxford, UK

Key Points:

- Identify 2120 creep events on the central San Andreas Fault and estimate their along-strike lengths.
- Creep event lengths range from sub-km to >10 km
- Existence of large events makes it likely that slip is driven by large-scale frictional weakening.

Corresponding author: Daniel Gittins, `daniel.gittins@earth.ox.ac.uk`

Abstract

Segments of many faults are observed to slip aseismically at the surface. On the central segment of the San Andreas Fault, aseismic slip accumulates largely in creep events: few-mm bursts of slip which occur every few weeks to months. But even though we have observed creep events worldwide since the 1960s, we still do not know how big most events are or which forces drive them. To address this uncertainty, we systematically identify creep events along the central San Andreas Fault and determine their along-strike rupture extents. We first use cross-correlation and visual inspection to identify events at individual creepmeters. With data from 18 USGS creepmeters, we identify 2120 records of creep events between 1985 and 2020. We then search for slip that is closely timed across multiple creepmeters. We identify 306 instances of closely timed slip, which could indicate 306 creep events that rupture multiple creepmeter locations. Through visual inspection and statistical analysis of timing, we identify a variety of creep event types, including single-creepmeter events, small (<2 km) events, medium-sized (3-6 km) events, large (>10 km) events, and events that rupture multiple fault strands. The existence of many large (>few-km) events suggests that creep events are not produced by small, rainfall-associated perturbations; they are more likely driven by complex or heterogeneous frictional weakening, and they may provide a window into the dynamics of larger-scale slip on the San Andreas Fault.

Plain Language Summary

The San Andreas Fault, CA, slips at the surface between San Juan Bautista and Cholame. This slip accumulates slowly or in bursts, known as creep events. Despite observations of creep events since 1966, we still do not know how large they are or what causes them to occur. Here we determine the length of creep events as this helps us understand more about how these events are created. If creep events are small, they may be caused by rainfall; however, if they are large, then they are likely self-driven. Using 18 USGS creepmeters, we identify the timing of creep events and determine their length. Between 1985-2020 we have identified 2120 creep events, some of which are recorded at multiple creepmeters, allowing us to determine their along strike-length. We identify five size ranges of our creep events: isolated events, small (<2 km) events, medium-sized (3-6 km) events, large events (>10 km), and events that occur on multiple fault strands events. These larger events are difficult to explain using conventional frictional theory and do not appear to result from rainfall. Therefore, understanding these events is important for determining the process that creates aseismic creep on faults.

1 Introduction

Some faults have been observed to creep at the surface since at least the 1960s. Detailed observations of creep were made following the 1966 Parkfield, CA earthquake and the 1968 Coachella Valley, CA earthquake (Bilham & Castillo, 2020; Titus, 2006). Since then, creep has been observed on many additional faults, including the San Andreas, Calaveras, and Hayward Faults in California (Evans et al., 1981; Lienkaemper et al., 2012; Steinbrugge et al., 1960); the North Anatolian Fault in Turkey (Ambraseys, 1970; Bilham et al., 2016); the Philippines Fault on the Island of Leyte (Duquesnoy et al., 1994); the Chihshang Fault, Taiwan (Lee et al., 2005; Thomas et al., 2014); and the Charman Fault, Pakistan (Fattahi & Amelung, 2016).

Here, we focus on the central creeping section of the San Andreas Fault in California. This 175 km-long segment between San Juan Bautista and Cholame (Figure 1) accumulates most of its slip aseismically (Titus et al., 2011). Two >100-km-long locked sections bound the creeping section. The locked section to the north of San Juan Bautista last ruptured in the 1906 M_w 7.9 San Francisco and 1989 M_w 6.9 Loma Prieta earthquakes, while the southern locked section south of Cholame last ruptured in the 1857 M_w 7.9 Fort Tejon earthquake

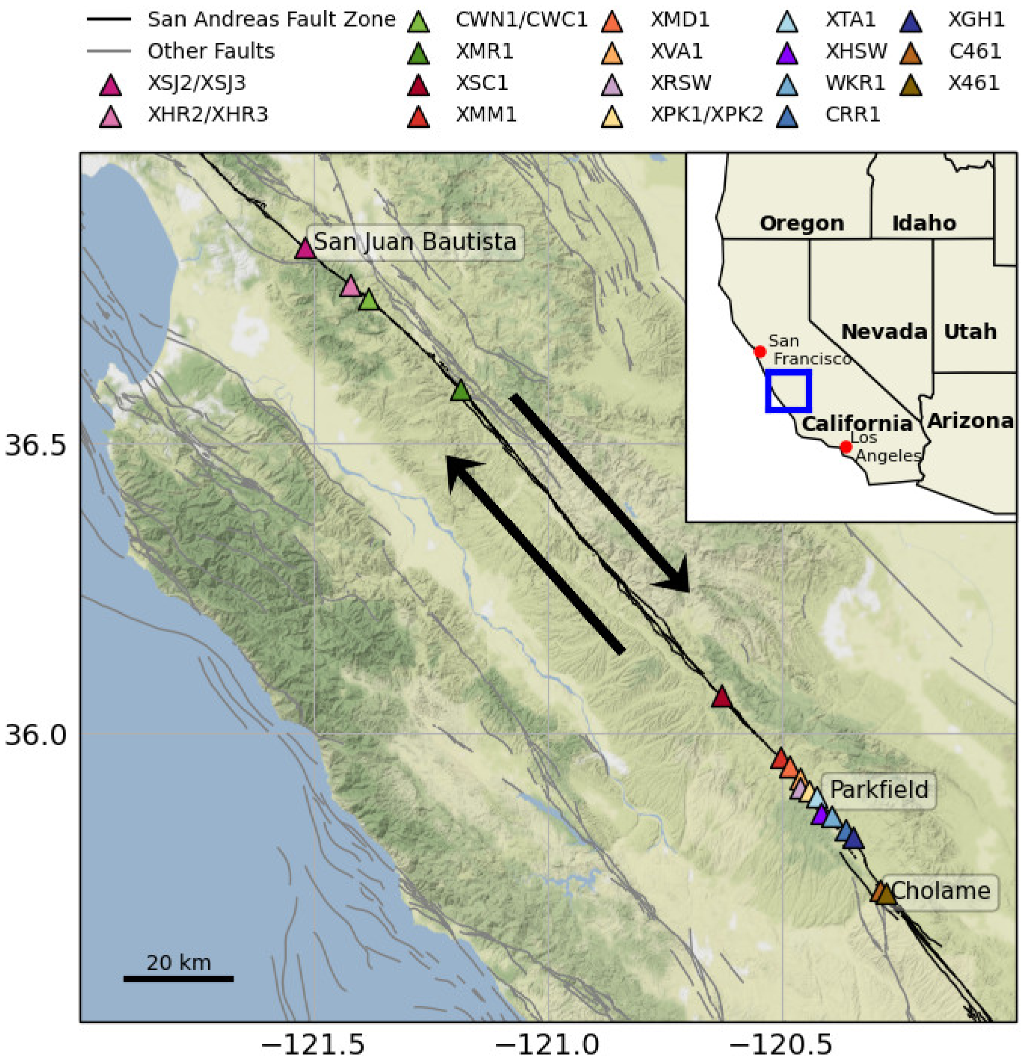

Figure 1. Map of the creeping section of the central San Andreas Fault (black) and other faults in central California (gray). The creepmeters are shown as colored triangles. Creepmeters have multiple numbers when an older creepmeter at the same location has been replaced. Faults plotted are from the USGS/CGS Quaternary faults and folds database (https://www.usgs.gov/natural-hazards/earthquake-hazards/faults).

(Ryder & Bürgmann, 2008; Titus et al., 2011). Smaller ($M \approx 6$) earthquakes also occur near the edges of the creeping section (Langbein et al., 2005). Yet, no major ($M \geq 7$) earthquake has ever been reported within this 175-km-long region (Toppozada et al., 2002).

But the long-term aseismic creep rate does vary along strike. It decreases from 30-33 mmyr^{-1} near the center to 10 mmyr^{-1} near Parkfield and Cholame (Titus, 2006; Ryder & Bürgmann, 2008; Titus et al., 2011; Jolivet et al., 2015). Many spatial and temporal variations of creep are well recorded along the San Andreas Fault's creeping section. Following the 1966 Parkfield earthquake, the region was heavily instrumented with creepmeters (e.g., Schulz, 1989), alignment arrays (e.g., Lienkaemper, 2006), GPS (e.g., Titus et al., 2011), trilateration networks (e.g., Lisowski & Prescott, 1981), and strainmeters (e.g., Gladwin et al., 1994).

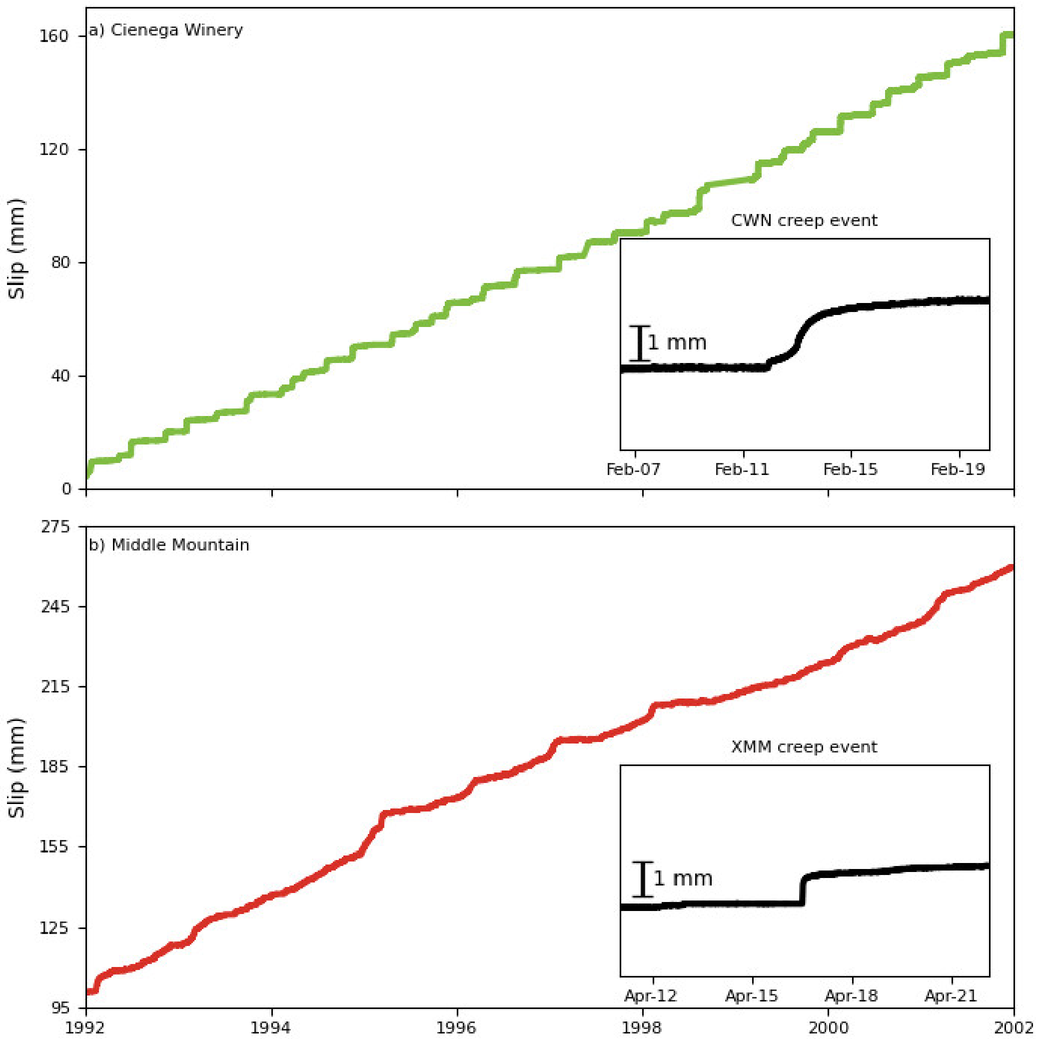

Figure 2. 10 years of slip at two creepmeter locations that show different creep event styles: a) Cienega Winery (CWN), and b) Middle Mountain (XMM).

The instrumental data revealed that creep on the central San Andreas Fault and other faults does not accumulate at a steady rate (Linde et al., 1996; Roeloffs, 2001; Jolivet et al., 2013; Rousset et al., 2016, 2019). On the central San Andreas Fault, creep accumulates mostly in small bursts of accelerated slip known as creep events (Figure 2). These creep events appear small and repetitive. They display mm to cm of slip, last hours to days, and recur at intervals of weeks to months (Gladwin et al., 1994; Schulz, 1989; Wei et al., 2013). There are larger creep events as well, with durations of weeks to years, but these larger events either accommodate small fractions of the surface slip or contain smaller bursts within them (e.g., Linde et al., 1996; Roeloffs, 2001). It appears that the small repetitive creep events play a dominant role in accommodating surface slip. But even though we know that small creep events are abundant and accommodate more surface slip on the 175-km creeping section, we do not know which fault zone processes cause creep events. We do not even know how *spatially* large most creep events are: how far the ruptures extend along strike or along depth.

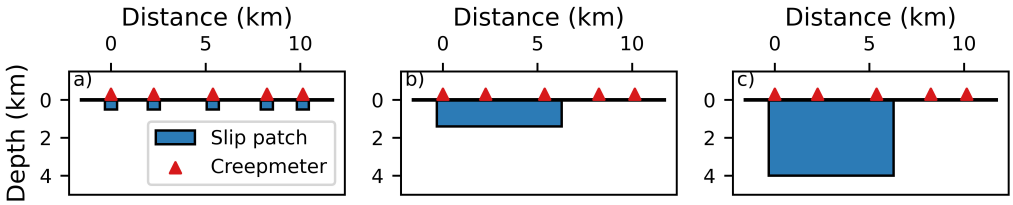

Figure 3. Three creep event size scenarios. a) Short, shallow ruptures. b) Long, shallow ruptures. c) Long, deep ruptures.

We do not know the spatial extent of most creep events because previous work has focused on a handful of larger events or repeated events at an individual creepmeter (Evans et al., 1981; Gladwin et al., 1994; Goulty & Gilman, 1978). Furthermore, slip at an individual creepmeter tells us only about the slip at a particular location; it does not tell how much of the fault is slipping. Previous estimates of the size of creep events vary widely. Some analyses have implied creep events are just short (640m), shallow ruptures (30-510m depth) (Figure 3a) (Gladwin et al., 1994; Goulty & Gilman, 1978) or long (6.6 km), shallow ruptures (510-1400m depth) (Figure 3b) (Evans et al., 1981; King et al., 1973). However, other evidence implies that creep events could be long and deep, rupturing to depths of 4km, perhaps all the way to the seismogenic zone (Figure 3c) (Bilham et al., 2016).

It is essential to know how large creep events are if we are to understand why they happen: to know what is happening in the fault zone that allows these episodic slow events. For instance, if creep events are small and shallow, one might imagine that the creeping San Andreas Fault is slip rate-strengthening, with a stable frictional rheology. Creep events could occur on a nominally stable fault if the fault receives some "kicks" in stress or pore pressure, perhaps from the stress perturbations by rainfall and atmospheric pressure (Helmstetter & Shaw, 2009; Kanu & Johnson, 2011). However, the "kick" hypothesis only seems plausible if creep events are shallow, occurring in a region with low normal stress that provides only modest resistance to acceleration. If creep events are large and deep, it seems more plausible to imagine that they are self-driven: driven by local frictional weakening. However, self-driven creep events are challenging to explain with conventional rate-strengthening or rate-weakening rheologies. To display the episodic but aseismic slip seen in creep events, a fault may require particularly-sized patches of rate-weakening material (e.g., Wei et al., 2013; Rubin, 2008; Liu & Rice, 2005; Skarbek et al., 2012; Yabe & Ide, 2017; Luo & Ampuero, 2018) or a more complex fault zone process such as shear-induced dilatancy (e.g., Segall et al., 2010; Segall & Rice, 1995; Iverson, 2005; Shibazaki & Iio, 2003; Leeman et al., 2018).

The different creep event sizes presented in Figure 3 also have different implications for the release of the strain that accumulates along the central creeping section. That moment deficit could be accommodated by a M_w 5.2 – 7.2 earthquake occurring every 150 years, on average (Maurer & Johnson, 2014; Ryder & Bürgmann, 2008; Michel et al., 2018). But depending on creep events' sizes, the moment deficit could be accommodated by occasional bursts of creep events (e.g., Khoshmanesh & Shirzaei, 2018b). If creep events often extend 10 km along strike to 4 km depth, a M_w 6.2 per 150 years deficit might be accommodated by a burst of 100 creep events occurring every 15 years. But if creep events are much smaller and shallower, they likely could not accommodate much in inferred moment rate deficits. Suppose creep events are typically 5 km long and 1 km deep. In that case, the observed moment deficit could be accommodated only by a burst of 800 creep events every 15 years.

In this study, we thus aim to take an important next step in unraveling the origin and role of creep events. We aim to determine the typical along-strike extent of creep events on the central San Andreas Fault. We first systematically identify creep events within the remarkable, decades-long USGS creepmeter record. Then we compare records from multiple creepmeters to characterize the ruptures' along-strike extents and determine if they are small, localized phenomena or large, segment-rupturing events.

2 Creepmeters and Creep Events

We use data from 18 USGS creepmeters along the creeping section of the San Andreas Fault (Figure 1) to investigate the along-strike length of creep events. Each creepmeter operated for at least nine years between 1985-2020. All creepmeters have sampling interval of 10-minutes except for Melendy Ranch (XMR1), which was upgraded to 1-minute sampling on 6$^{\text{th}}$ September 2018 by the USGS and R.Bilham.

The creep events we analyze are mostly well recorded. They appear in the data as accelerated bursts of slip (Figure 2). These bursts of slip can be simple (Figure 2b) or have multiple steps (Figure 2a) that could reflect a migrating slip location (Bilham & Behr, 1992; Gladwin et al., 1994).

However, there are also many steps in the data that are not creep events. Some steps result from small nearby earthquakes, while others arise because of friction within the creepmeter instrumentation (Bilham & Castillo, 2020). These steps are usually distinguishable from creep events because they occur abruptly, while creep events typically last hours or days.

3 Identifying Creep Events at Individual Creepmeters

In order to constrain creep events' spatial extent and timing, we first needed to find the events in the data. The creep events we are interested in are readily identifiable via visual inspection, but visually examining decades of creepmeter records would be time-consuming. So we identified the creep events at each creepmeter using an automated approach to obtain initial potential detections. Then we used visual inspection to refine the catalog.

3.1 Automated Detections

A full in-depth description of our automated detections is presented in Supplementary Text S1. Here we detail the main processing steps undertaken by our detection scheme.

We began by identifying times of potential creep events: times when the creepmeter record is similar to a template creep event and when there is a significant slip.

For this analysis, we first prepared the data. We interpolated the creepmeter record to ensure that the data were spaced evenly at 10-minute intervals, removed a long-term trend, and bandpass filtered to focus on variations between 2 h and 5 d: the dominant periods of the creep events. The black curves in Figure 4 a & b illustrate a creep event record before and after filtering. We then picked one template creep event for each creepmeter (green curve in Figure 4b). One creepmeter is an exception; we used two templates for the Melendy Ranch (XMR1) creepmeter, as the data's sampling frequency increased after it was updated.

Next, we conducted a rough automated detection by cross-correlating the template creep events with the creepmeter records. We identified peaks in the cross-correlation that exceeded a creepmeter-dependent threshold between 0.05 and 0.2, allowing only one peak per 40-minute interval (Figure 4c). The thresholds for detection were set relatively low, allowing

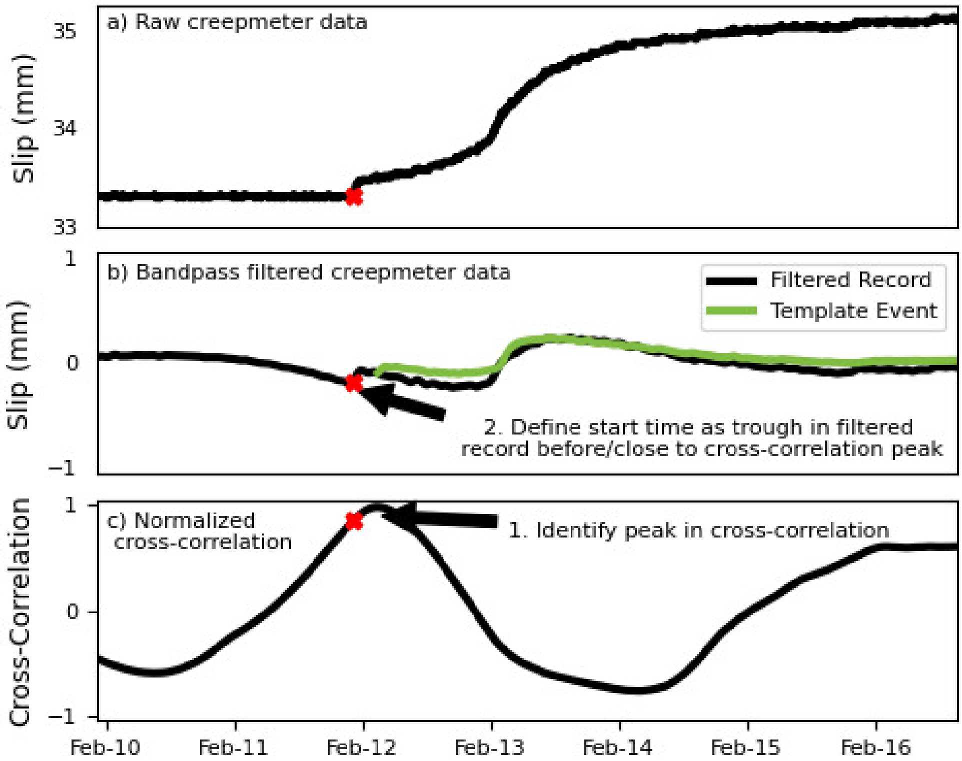

Figure 4. Processing stages of the automated detection. a) Raw creepmeter data from Cienega Winery (CWN) showing a creep event on 11^{th} February 1994. b) The same creep event bandpass filtered between 2 h and 5 d (black line), along with the template creep event (green line). The template has been aligned with the data according to the peak of the cross-correlation time series shown in panel (c). The red cross in all panels indicates the estimated creep event start time, taken as the time of the trough in the filtered data in panel b.

for many false positives so that we could identify creep events with shapes that varied from the template.

After identifying the potential creep events, we estimated their start times by examining the running average of the slip in hourly windows just before and after the cross-correlation peak. We identified the potential event start as the time when this hourly slip first appears significant: when it exceeds a noise-based threshold value. Then we refined the start times using a feature of the filtered creep record: a distinct trough at the start of creep events (Figure 4b). We used the time of the nearest trough as our automated estimate of the potential creep events' start times (red cross in Figure 4).

To estimate the potential creep events' end times, we examined the running average of the slip in overlapping daily windows following the start time. End times were estimated as the first time after the event began, where this daily slip fell below a noise-based threshold.

Once we had end time estimates, we could calculate the slip in each potential creep event. We subtracted the slip at the start time from the end time. This simple difference provides the best estimate of the slip in the identified time period, given that the noise in the creepmeter record has a random walk character at periods longer than 1 hr (e.g., Langbein et al. (1993); Langbein and Johnson (1997)).

The slip estimates provided a useful way of removing tiny events, most of which result from instrumental resolution or friction within the creepmeters. We removed detections when they had slip less than 1% of the median slip from the largest 10% of creep event detections at each creepmeter.

In our last automated step, we merged events as necessary. Some creep events include multiple accelerations, and those can be detected as multiple creep events. We merged the detections if the start and end times of two potential creep events were the same or overlapped.

Finally, we visually inspected all of the potential creep events to ensure no false positives are carried forward into further work. We manually corrected each start time based on a visual inspection of the data.

3.2 Results

With our automated and manual analysis, we identified 2120 creep events at 18 creepmeters. This event catalog is provided in Supplementary Section 2. Figure 5 shows some of the patterns evident in this catalog: the number of events at each creepmeter, as well as the events' median slip and duration. There is an anti-correlation between the number of creep events at each creepmeter (Figure 5a) and the slip (Figure 5b) and duration (Figure 5c) of those events. This summary confirms our inferences from visually examining the record: that some fault sections slip in numerous creep events, each with small slip (e.g., Middle Mountain, XMM (Figure 2b)), while others slip less frequently, in creep events with large slip (e.g., Cienega Winery, CWN (Figure 2a)).

Using our creep event catalog, we have produced a booklet (Supplementary Section 3) displaying all the creep events we observe and the creep recorded on other creepmeters at the time of the event. This booklet was useful in identifying creep events that may rupture the surface at more than one creepmeter (Section 4.3).

4 Identifying Correlated Events Between Creepmeters

An initial visual analysis of the creep event records suggested that some of the creep events span relatively long distances along strike. For instance, the event in Figure 6 is observed at two creepmeters separated by 4 km. In this section, we describe how we used the closely timed event detections to determine the spatial extent of creep events. We describe how we determined the frequency of multi-creepmeter events, accounted for rainfall-induced coincidences, and visually examined identified ruptures. We summarize the common creep event behaviors identified with this analysis in Section5.

4.1 Estimating the Frequency of Multi-creepmeter Ruptures

It is clear from the records in Figure 6 that creepmeters 4 km apart sometimes display slip accelerations at close times, and it would seem plausible that the accelerations result from a single, >4-km-long creep event. However, it is also possible that the closely timed accelerations are just a coincidence or just a rare large creep event. Our next task, then, was to determine the fraction of creep events observed at one creepmeter that have a closely timed event at another.

We examined the frequency of closely timed creep events at all pairs of creepmeters. We first isolated the period in which both creepmeters were operational, excluding the period between 28$^{\text{th}}$ September 2004 and 1$^{\text{st}}$ January 2006 on southern creepmeters because this interval is affected by the 2004 $M6$ Parkfield earthquake. We defined one creepmeter in each pair as the main creepmeter. For each creep event on this main creepmeter, we identified

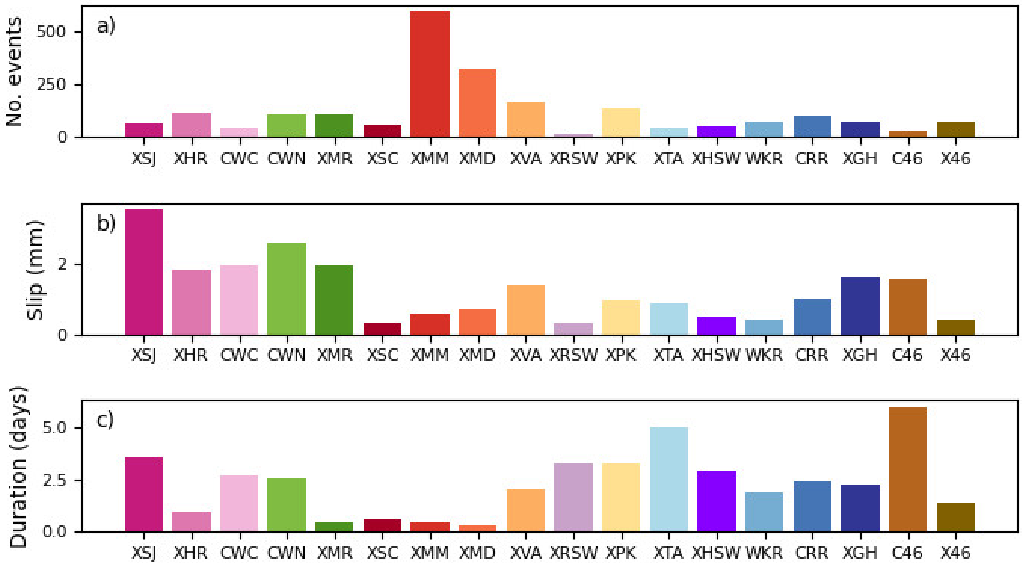

Figure 5. Properties of the creep events at each creepmeter. a) Number of detected events. b) Median creep event slip. c) Median creep event duration.

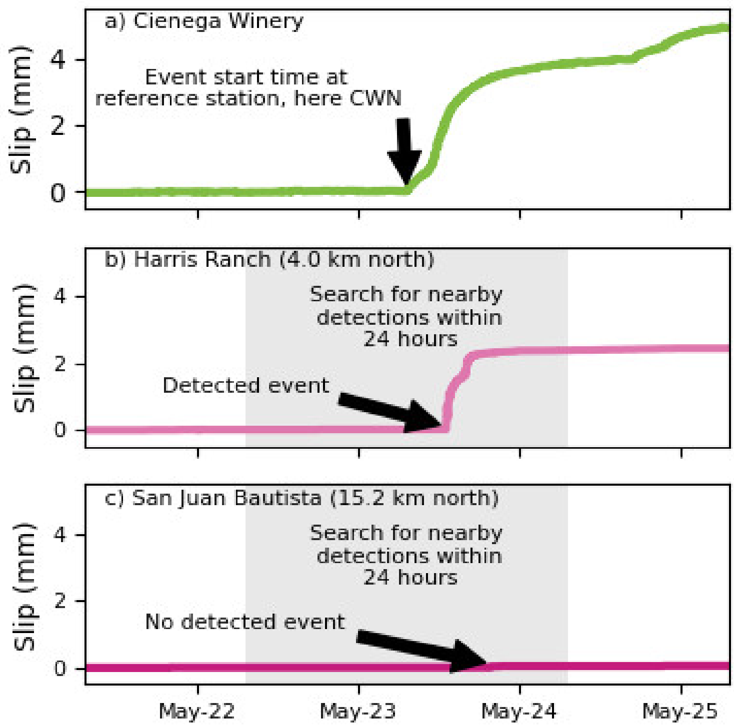

Figure 6. Creep records for the 21 to 26th May 2016 at (a) Cienega Winery (CWN), (b) Harris Ranch (XHR), and (c) San Juan Bautista (XSJ). The figure illustrates our approach to detecting closely timed events. For each event at Cienega Winery (panel a), we search for events at (b) Harris Ranch and (c) San Juan Bautista that occur within 24 hours of the Cienega Winery event (gray regions in panels b and c).

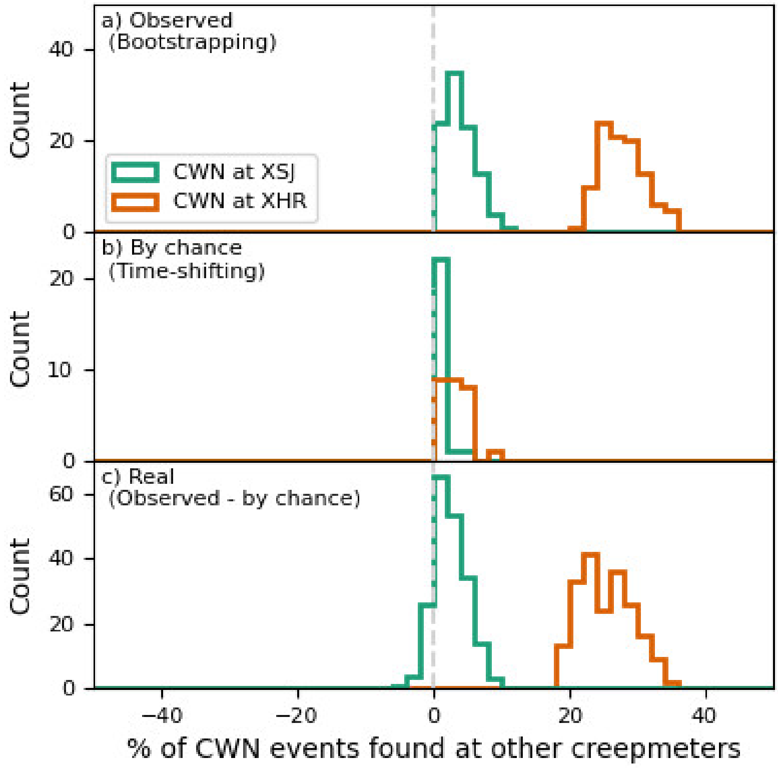

Figure 7. a) Probability distributions of the percentage of CWN creep events observed at XHR (orange) and XSJ (green) within 24 hrs, based on bootstrapping. b) Probability distributions that a CWN event would coincide with an XHR or XSJ event by chance: if events were randomly timed. c) The distributions in (a) minus the distributions in (b): probability distributions on the percentage of CWN events that observed at XHR and XSJ within 24hrs for a physical reason.

the closest event on the second creepmeter and noted the time between the two. Since creep events typically last hours to days, we were particularly interested in when the time between creep events was less than 24 h. We calculated the percentage of creep events observed at the main creepmeter that occur within 24 h of a creep event at the second creepmeter.

Next, we calculated the uncertainty on this percentage of closely timed creep events. We bootstrapped the data and recomputed the percentage using various subsets of the creepmeter records. We divided the main creepmeter record into years, and in each recomputation, we picked the same number of years as in the original record, but with replacement, and calculated the percentage of these creep events within 24 h of events at the second creepmeter. This bootstrapping allowed us to estimate a probability distribution on the percentage of events at the main creepmeter that occur within 24hrs of an event at the second creepmeter. The 15th to 85th percentiles of the orange histogram in Figure 7a tells us, with 70% probability, that 24.3 to 31.5% of CWN events are within 24 hrs of an event at XHR.

However, closely timed events are not necessarily physically meaningful; some of the XHR events could occur just before or after CWN events by chance. To determine how many events could be closely timed by chance, we redo our analysis after randomly shifting the times of creep events at the main creepmeter by 1 to 35 years. In each reanalysis, we shifted all of the creep event times by the same amount, looping the times of events shifted beyond the end of the record back through the start. With this constant shift, we were able to maintain the temporal spacing and thus the recurrence statistics of the creep events. Further, we use time shifts that are multiples of 1 year to preserve the seasonality of the creep event timing. This time-shifting creates a distribution (Figure 7b) that encompasses the percentage of creep events recorded on two creepmeters by chance and unrelated.

To estimate the number of "real" closely timed events – those that are not by chance, we subtracted the by chance distribution (Figure 7b) from the bootstrapped observed distribution (Figure 7a). The probability distribution of these real closely timed events is shown in Figure 7c, in green for the CWN-XSJ pair and orange for the CWN-XHR pair. In Figure 7c the CWN-XSJ distribution crosses 0% (vertical dashed grey line) and has a 70% confidence interval of 0 to 5.1%, meaning that coincidentally timed events are likely to be unrelated. In contrast, the CWN-XHR distribution is well above 0%, with a 70% confidence interval of 21.3 to 29.1%, indicating that coincidentally timed events are related.

The percentages of events for of each creepmeter pair are presented in Figures S1-S17. Certain pairs are discussed in more detail in Section 5.

4.2 Removing Short-term Rainfall Effects

Our results suggest that for many pairs of creepmeters, events are closely timed more often than one would expect by chance. However, these temporal coincidences do not necessarily imply that a single creep event ruptures from one creepmeter to the other; there could be two small events, one near each creepmeter (e.g., Figure 3a). These two small events could be closely timed because they both respond to atmospheric or hydrological signals. The long-timescale components of seasonal hydrological signals are already accounted for in our by-chance distributions, as we used only time shifts that were multiples of a year. Here, however, we probe the shorter-timescale influence of rainfall on multi-creepmeter creep events.

To probe the rainfall effect, we again recomputed our closely timed event percentages (Section 4.1), but with few modifications. We used rainfall records from the four NOAA weather stations to identify creep events at the main creepmeter preceded by a 3, 7 (orange in Figure 8) or 14-day (red in Figure 8) interval that included rainfall. These events were then removed from the main creepmeter before bootstrapping (Figure 8a) and shifting (Figure 8b) of the creep event dataset at the main creepmeter. We then computed the subtraction as before to determine the percentage of physically related creep events in following wet and dry periods (Figure 8c).

In this reanalysis, we do not use all creepmeter pairs. We consider only pairs that showed significant correlation to one another before rainfall considerations. If both creepmeters in the pair are triggered by rainfall, we would expect to see a reduction in correlation when we remove events that follow rainfall. Often, however, we see a minimal change in the correlation. For instance, the similarity of the blue to red histograms in Figure 8c suggest that the closely timed creep events at XMM and XMD are caused by something other than rainfall—perhaps slip at depth.

We summarize how excluding rainy intervals influences or does not influence the percentage of closely timed creep events for more pairs of creepmeters in the Section 5. Those quantified influences are enough to determine the significance or lack of significance in the closely timed event percentages. Here, however, we also briefly consider how rainfall influences creep event timing. To slightly better understand the influence of short-timescale rainfall, we probed the number of creep events at "random" times at the second creepmeter (Figure 8d). To preserve the seasonality, we created random times by shifting the times of the main creepmeter events by multiples of a year. We then excluded events preceded by 3, 7, or 14-day intervals with rainfall before computing the percentage of times within 24 hours of

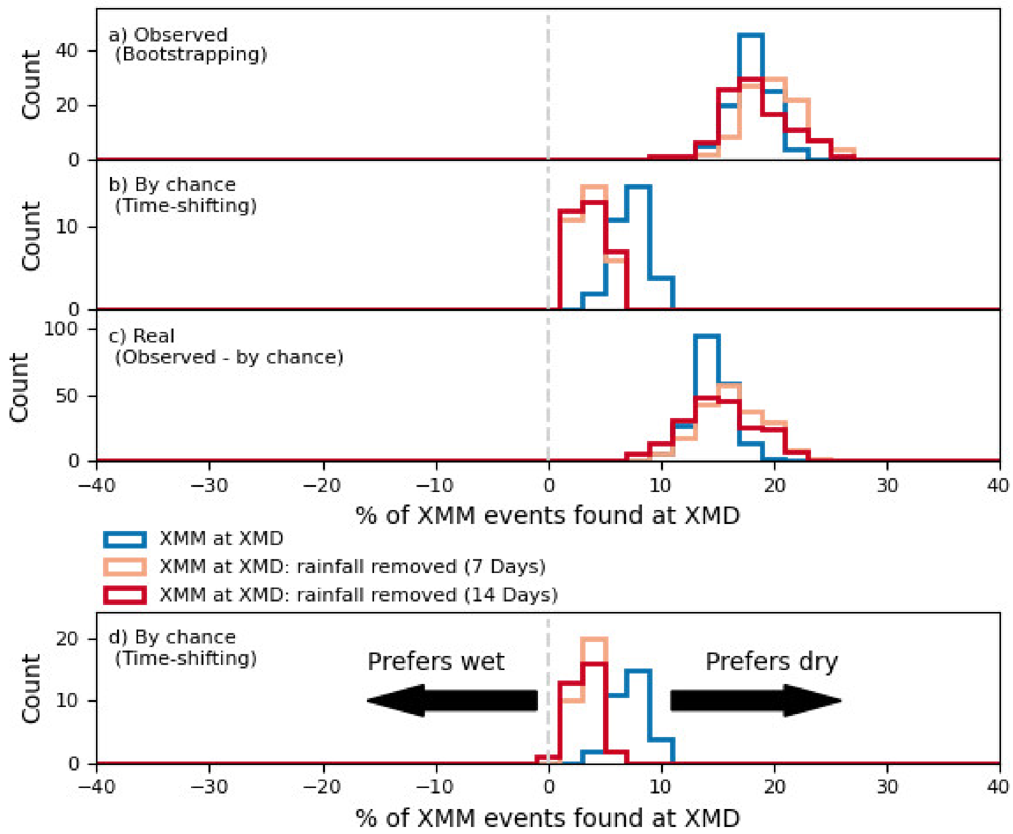

Figure 8. (a-c) Probability distributions on the percentage of XMM events observed at XMD. Panels a-c are as in Figure 7, with the observed, by chance, and real percentages, but the three histograms in each panel illustrate the effect of removing rainy intervals. The blue histograms use all XMM events in the comparison while the orange and red histograms use only XMM events that follow 7 or 14-day periods without rain. d) The percentage of XMM events observed at XMD by chance, as in panel b, but when XMD events preceded by rainfall are removed. The reduced percentage suggest that XMD events are more common in rainy intervals.

a creep event at the second creepmeter (Figure 8d). These new time-shifted distributions allowed us to determine if certain creepmeters preferred to slip in wet or dry conditions (given the seasonality of the main creepmeter). For instance, it appears from Figure 8d that the creepmeter at Middle Ridge (XMD) prefers to slip in wet conditions; the percentage of times with creep events decreases when rainy intervals are removed. We do not discuss this further, however the relevant results are presented in the supplement (Figures S19-S25).

4.3 Detecting Long Creep Events by Visual Inspection

Having determined the frequency of multi-creepmeter events and assessed the affects of rainfall, We next use our event detections to inspect coincidently timed creep events at multiple creepmeters visually. Using our creep event catalog, we identify all the creep events at each creepmeter that occur within 24 hrs of a creep event at any other creepmeter to produce a subsection of our catalog that only contains these events. This subsection of events contains 306 potentially large creep events that rupture two or more creepmeters within 24 hrs, made up of 719 different individual detections from our creep event catalog. We present examples of different sized creep events in Section 5 and provide figures illustrating all of the multi-creepmeter events in the second supplementary creep booklet.

Visual inspection also allowed us to probe where slip happens in a creep events: on the surface or at depth. We find that some creep events appear to rupture more at depth than at the surface, sometimes skipping creepmeters along a sequence (Section 5.4). We discuss this furhter in Section 7.2.

5 Summary of Creep Event Behaviors

The creep event correlation described above reveals that many creep events rupture several kilometers along the fault strike. But other creep events appear short, perhaps less than 1 km long. By analyzing over 2000 creep events, we are able to identify a variety of creep event behaviors. Here we describe the five most common creep event types: (1) isolated events, (2) small (<2-km) events recorded at two creepmeters, (3) 5-km events recorded at multiple creepmeters, (4) long (10 to 30-km) propagating events, and (5) multi-strand ruptures.

5.1 Isolated Events

A few creepmeters in this study appear to show only isolated creep events: events that are recorded at no other creepmeters.

5.1.1 San Juan Bautista (XSJ)

The creepmeter at San Juan Bautista (XSJ) displays isolated, repetitive 3 to 4-mm events every few months, which were previously analyzed by Gladwin et al. (1994). One of these isolated events is shown in Figure 9a. The XSJ events show weak to minimal correlation in timing with the closest neighboring creepmeters. Although 0.5 to 8.5% of XSJ events are recorded at Cienega Winery (CWN) 15.3 km southeast according to 70% confidence intervals, 70% confidence intervals overlap zero and have a maximum of 2.0% for a closer creepmeter located 11.2 km southeast (Figure 9b).

In each of the right hand panels of Figures 9-12, we have designated one relevant creepmeter as the 'main' creepmeter. The plots show the median percentage of events at the 'main' creepmeter that are observed at every other creepmeter, with 70% confidence intervals.

5.1.2 Melendy Ranch (XMR)

The creepmeter at Melendy Ranch (XMR) displays 2-mm events (Figure 9c) every few months that are recorded at no other creepmeter (Figure 9d). However, this creepmeter is far from its neighbors: 24.6 km southeast of Cienega Winery (CWN) and 77.32 km northwest of Slacks Canyon (XSC). Nevertheless, it is interesting to note that this creepmeter is situated above a locked patch identified by Jolivet et al. (2015). The locked patch could prevent creep events from rupturing into and out of the XMR area.

5.1.3 Gold Hill (XGH)

The creepmeter at Gold Hill (XGH) also displays isolated events (Figure 9e). These events are more intriguing than those at San Juan Bautista (XSJ) and Melendy Ranch (XMR) because XGH is just 2.2 km southeast of the Carr Ranch (CRR) creepmeter, yet there is no evidence of creep events that rupture both locations (Figure 9f). Indeed, on timescales of months to years, these locations seem to have anticorrelated slip rates. For instance, when the slip rate at CRR increased in September 1994, the slip rate at XGH decreased. Moreover, when the slip rate at CRR decreased between 2016 and 2017, the slip rate at

XGH increased. This anti-correlation in slip was noted by Roeloffs (2001), who suggested that slip accumulates at one location before reaching a threshold that allows slip at the other location.

5.2 Small Events (2 km or Less) Recorded at Two Creepmeters

Some creepmeters record events that coincide in time with events at creepmeter a short distance away.

5.2.1 Middle Mountain (XMM) - Middle Ridge(XMD)

The fault section between Middle Mountain (XMM) and Middle Ridge (XMD) is around 8 km north of Parkfield. These two creepmeters are 2.26 km from each other, 14.2 km from creepmeters farther north, and 2 km from creepmeters farther south. Both creepmeters record large numbers of <1-mm creep events, which occur every few weeks (see Figure 5a). Our analysis of coincidently timed events implies that many of these small creep events rupture both creepmeter locations (Figure 10a). 70% confidence intervals suggest that 12.9 to 16.3% of XMM events are also recorded at XMD, and 25.9 to 31.9% of XMD events are observed at XMM (Figure 10b).

When creep events with rainfall in the 7-14 days before the event are removed, the percentage of XMM events found at XMD and vice versa does not change significantly. When events preceded by a 14-day interval with rainfall are removed, 11.8 to 19.0% of XMM events are observed at XMD, and 24.4 to 34.7% of XMD events are observed at XMM. Combining these percentages with the observation that XMM and XMD have opposite responses to rainfall (Figure S19g & S19h) implies that correlated events recorded at these two creepmeters are not due to atmospheric effects; instead, their correlation is due to a slip at depth on the fault.

5.2.2 Highway 46 creepmeters (C46 - X46)

The southernmost pair of creepmeters is situated near Highway 46, 10 km south of the cluster of creepmeters around Parkfield. Creepmeters C46 and X46 are 1.27 km apart and record fewer events than Middle Mountain (XMM) and Middle Ridge (XMD); 0.4 to 1.6-mm events occur around 1-2 times a year. However, many of the recorded creep events rupture both locations (Figure 10c). 70% confidence intervals suggest 50.0 to 66.7% of creep events at C46 are observed at X46, and 47.1 to 64.8% of X46 events are observed at C46 (Figure 10d).

When creep events with rainfall in the 7-14 days before the event are removed, the percentage of C46 events at X46 increases. When events with rainfall in the 14 days prior are removed, 40 to 80% of C46 events are found at X46, and 100% of X46 events are found at C46 (Figure S20), which may arise from slip at depth. The picture of this section is not fully clear as both C46 and X46 prefer to slip in wet conditions (Figure S20g & S20h). This would suggest that some of the correlation here is rainfall induced, however there is still some evidence for slip at depth, given the percentage of correlated events goes up when rainfall is removed.

5.3 Medium-sized Events (3-6 km) Recorded at Two or Three Creepmeters

The next most frequently observed type of creep events are 3 to 6 km long and are typically observed at two or three creepmeters. These 5-km-long events are found at multiple locations along the fault from Cienega Winery in the north to Highway 46 in the south.

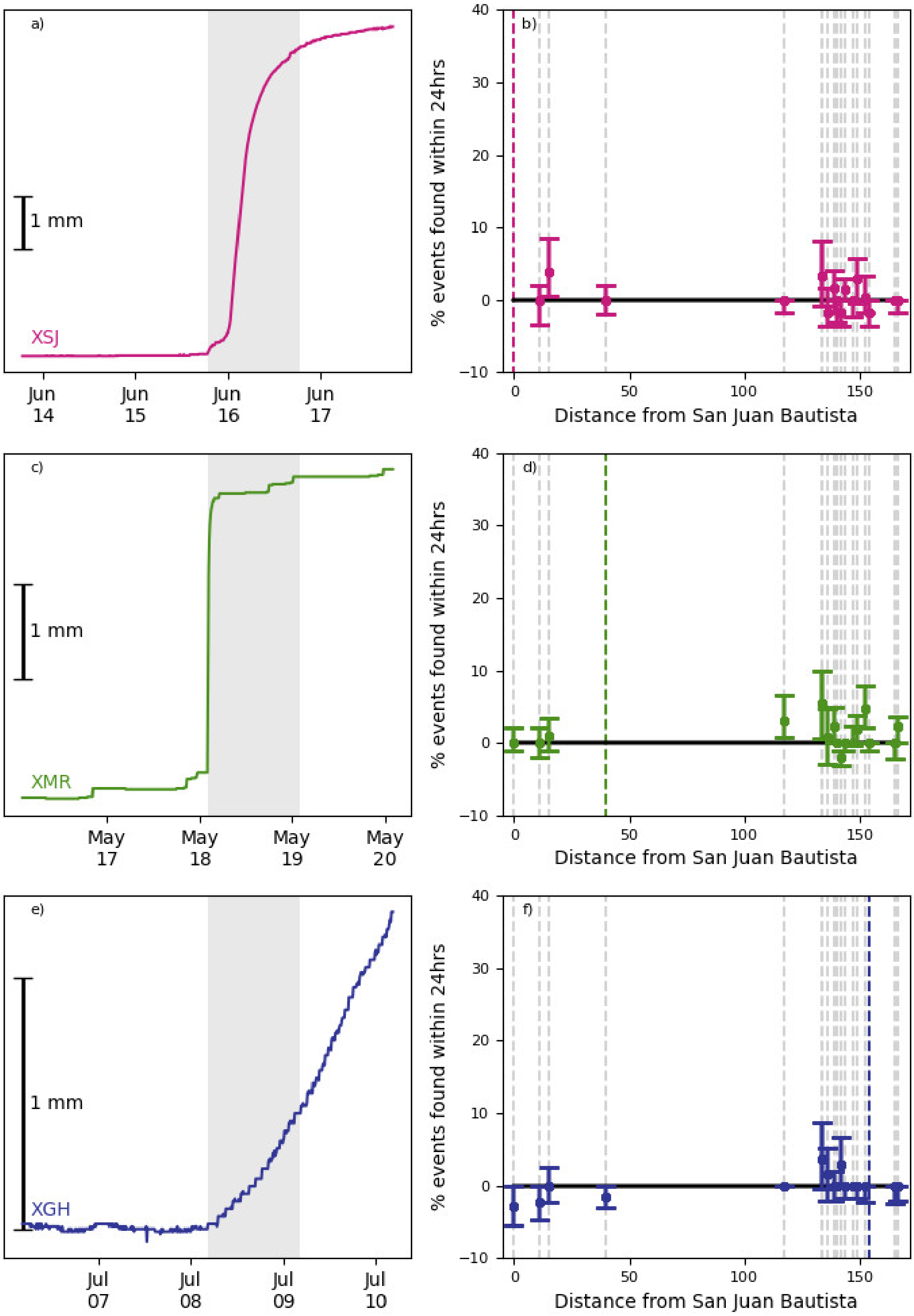

Figure 9. Creep events and percentage of events observed at other creepmeters for isolated creep events at XSJ, XMR, and XGH. a) Creep event at XSJ on 15^{th} June 1993. c) Creep event at XMR on 18^{th} May 1993. e) Creep event at XGH on 8^{th} July 1991. b), d) and f) indicate the percentage of events XSJ, XMR, and XGH events found at other creepmeters, with 70% confidence intervals. Vertical colored lines in b), d) and f) mark the location of the creepmeter.

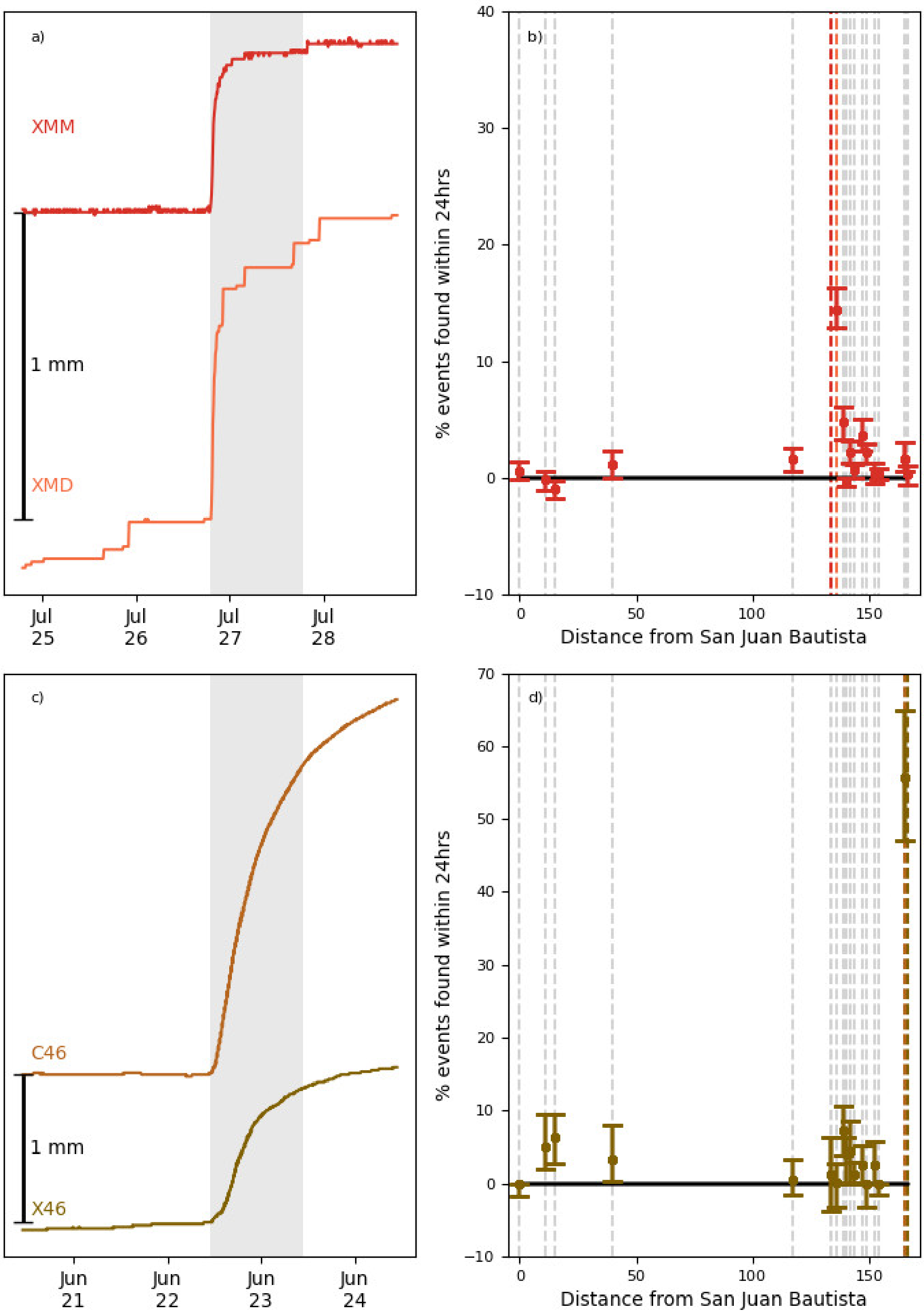

Figure 10. Small creep events from the XMM - XMD and Highway 46 (X46 & C46) areas and percentage of events observed at other creepmeters for XMM and X46. a) Creep event at XMM and XMD on 26^{th} July 1991. c) Creep event at X46 and C46 on 22^{nd} June 2015.b) and d) indicate the percentage of XMM and X46 events found at other creepmeters, with 70% confidence intervals. Vertical colored lines in b) and d) mark the location of the creepmeters in a) and c).

5.3.1 Harris Ranch (XHR) - Cienega Winery (CWN)

The northern end of the creeping section between Harris Ranch (XHR) and Cienega Winery (CWN) hosts a series of creep events that have an along-strike length of at least 4 km (Figure 11a). Events at CWN and XHR are typically 2-2.5 mm and occur every few months. 70% confidence intervals suggest that 17.4 to 26.6% of creep events recorded at XHR are also recorded at CWN, and 21.3 to 39.1% of CWN events are observed at XHR (Figure 11b).

When creep events with rainfall in the 7 days before the event are removed, the percentage of XHR events observed at CWN and vice versa does not change significantly, with 16.3 to 28.5% of XHR events recorded at CWN and 20.8 to 32.0% of CWN events observed at XHR. And if creep events with rainfall in the previous 14 days are excluding, the percentage of events rupturing both stations actually increases. If events with rainfall in the 14 days before the event are removed, 29.6 to 47.6% of XHR events are observed at CWN, and 28.0 to 48.7% of CWN events are observed at XHR (Figure S21). The relationship between XHR, CWN and rainfall is discussed in more detail in Section 6.3.

5.3.2 Middle Mountain (XMM) - Middle Ridge (XMD) - Varian (XVA)

Farther south, the fault section between Middle Mountain (XMM) and Varian (XVA) also hosts 5-km-long events. As noted in Section 5.2.1, creep events rupture between XMM and XMD frequently. However, not all of the events in this fault section are simple, 2-km ruptures. Some events continue rupturing farther south to reach XVA (Figure 11c). 70% confidence intervals suggest that XVA events coincide with events at both XMM and XMD. 3.3 to 6.1% of events at XMM are observed at XVA, and 12.9 to 23.3% of XVA events are observed at XMM (Figure 11d). Further, 5.3 to 9.8% of XMD events are observed at XVA, and 11.0 to 18.8% of XVA events are observed at XMD (Figure 11d). Three-creepmeter ruptures can start at any of these stations. However, ruptures are most commonly seen first at XMD; the creep events may preferentially nucleate near XMD (Roeloffs et al., 1989; Rudnicki et al., 1993).

We note, however, that some apparent XMM-XVA or XMD-XVA rupture could arise because coincident creep events are triggered by rainfall. When creep events that are preceded by a 7-day interval that includes rainfall are removed, the percentage of XVA events observed at XMM decreases to 6.6 to 21.8%, and the percentage of XMM events observed at XVA decreases to 1.3 to 5.1%. The percentage of closely timed XMD-XVA events also decreases. 4.9 to 17.5% of XVA events observed at XMD and 3.2 to 7.3% of XMD events observed at XVA. When events with rainfall in the 14 days prior are removed, the percentage of XVA events at XMM reduces to 1.0 to 16.7%. The percentage of XMM events at XVA becomes 0 to 4.4%, implying that they may be unrelated. However, the percentages for XMD and XVA remain roughly constant when 7 or 14 days of rainfall are removed. These reductions in percentages imply that XMM and XVA events may be unrelated when longer-term rainfall is considered; however, the relation between XMD and XVA remains. These relations suggest that there are often events that rupture from XMD to XVA (a distance of 3.1 km) but do not always rupture up to XMM and may require atmospheric perturbations to do so.

5.3.3 Varian (XVA) - Parkfield (XPK) - Taylor Ranch (XTA)

In the last subsection, we discussed creepmeters that observed creep events to the north of Varian (XVA). However, XVA also hosts events that are only observed to the south, at the Parkfield creepmeter (XPK, 2.9 km away) and potentially at the Taylor Ranch creepmeter (XTA, 4.8 km away) (Figure 11e). 70% confidence intervals suggest that between 13.2 and 20.5% of XVA events are observed at XPK, and 15.5 to 25.3% of XPK events are observed at XVA (Figure 11f). These numbers imply that many events rupture the 2.9 km from XVA to XPK. Many events also rupture the 1.9 km from XPK to XTA; 70% confidence intervals suggest that 5.1 to 10.0% of XPK events are recorded at XTA and that 20.3 to 34.9% of XTA events are observed at XPK (Figure S10 - S11). These percentages are minimally affected by removing times with rainfall.

However, even though XVA-XPK and XPK-XTA events are common, few to zero events rupture the entire 4.8 km from XVA to XTA; 70% confidence intervals suggest that 0 to 2.6% of XVA events are found at XTA and that 0 to 9.1% of XTA events are found at XVA (Figure 11f). When rainfall is removed, the percentages of XVA events at XTA and vice versa are reduced slightly, with the lower bound remaining at 0%, meaning that the coincidently timed XVA and XTA events may either be unrelated or driven by rainfall. The lack of closely timed events at XVA and XTA suggests that creep events along this region prefer to slip in two sections: XVA to XPK (2.9 km) or XPK to XTA (1.9km). Creep events rupture the 4.8 km from XVA to XTA less frequently or perhaps not at all.

5.3.4 Roberson Southwest (XRSW) - Hearst Southwest (XHSW)

Medium-sized multi-creepmeter ruptures may also be present on secondary strands of the San Andreas Fault: in a 6.4-km stretch between Roberson Southwest (XRSW) and Hearst Southwest (XHSW). Events on this secondary strand are less frequent than on the main strand, but we still observe closely timed creep events (Figure 11g). 70% confidence intervals suggest that 4.3 to 31.2% of XRSW events are observed at XHSW, and 0.0 to 10.3% of XHSW events are observed at XRSW (Figure 11h). The statistics are somewhat difficult to interpret because XRSW displays just 11 creep events, and that number is reduced by 50% when we remove creep events preceded by rainfall (Figure S18). So we simply note here that the XHSW-XRSW statistics marginally suggest that several creep events could rupture the 6 km between these creepmeters.

5.4 Large Events (10 km or more), Sometimes Skipping Creepmeters

The potential 6-km creep events between XHSW and XRSW are not the longest creep events we observe. Some closely timed creep events suggest ruptures that span 10 or even 30 km.

5.4.1 10 km Events

The 10-km events occur in the region we discussed in sections 5.3.2 and 5.3.3, between Middle Mountain (XMM) and Taylor Ranch (XTA), including XMD, XVA, and XPK. Two-creepmeter 2 to 5-km events are frequently observed in this region. But in September 2000, a large creep event was recorded at all five creepmeters (Figure 12a). Such closely timed slip at these creepmeters seems unlikely to be a coincidence or rainfall-induced; the September event was preceded by 104 days without rainfall. However, we only observe this 10-km XMM to XTA events once suggesting such events are rare; 70% confidence intervals suggest that 0 to 1.2% of XMM events are observed at XTA, and 0 to 15.3% of XTA events are observed at XTA.

The 8.2 km-long XMM to Parkfield (XPK) section ruptures more frequently. 70% confidence intervals for this section suggest that 1.2 to 3.1% of XMM events are observed at XPK, and 5.1 to 14.6% of XPK events observed at XMM (Figure 12b). Some of the closely timed events could be induced by rainfall, however. When creep events with rainfall in the 7 days prior are removed, 0.4 to 3.8% of XMM events are observed at XPK, and 3.9 to 18.4% of XPK events are observed at XMM. Moreover, if events with rainfall in the 14 days prior are removed, the relationship between XMM and XPK has at least a 15% chance of being explained by atmospheric perturbations.

Assuming that the closely timed slip at XMM and XPK do reflect 8-km-long creep events, it is interesting to note that even when creep events appear to rupture from XMM to XPK,

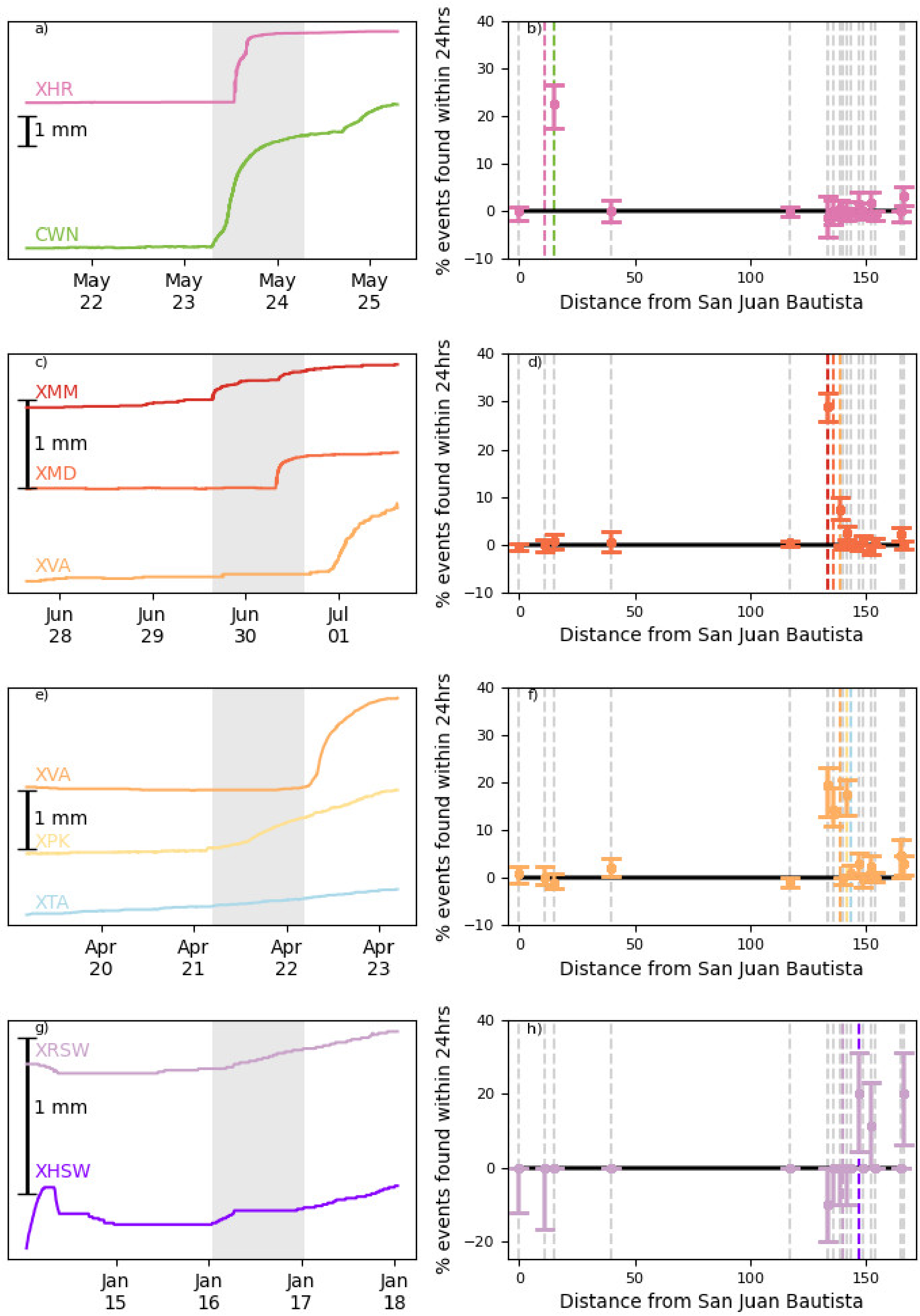

Figure 11. Medium-sized creep events from the XHR - CWN, XMM - XVA, XVA - XTA areas and the Southwest trace (XRSW - XHSW) and percentage of events observed at other creepmeters for XHR, XMD, XVA, and XRSW. a) Creep event at XHR and CWN on 11^{th} - 12^{th} February 1994. c) Creep event at XMM, XMD and XVA on 29^{th} - 30^{th} June 2014. e) Creep event at XVA, XPK and XTA on 21^{st} - 22^{nd} April 2008. g) Creep event at XRSW and XHSW on 16^{th} January 1993. b), d), f), and h) indicate the percentage of XHR, XMD, XVA, and XRSW events found at other creepmeters, with 70% confidence intervals. Vertical colored lines in b), d), f), and h) mark the location of the creepmeters in a), c), e) and g) respectively.

they sometimes do not appear at the creepmeters in the middle (XMD and XVA). The lack of intermediate surface rupture suggests that the creep events commonly rupture at depth and sometimes do not reach the surface.

5.4.2 Potential 31-km Events: Slacks Canyon (XSC) - Work Ranch (WKR)

Some of the largest creep events that we seem to observe are those that propagate between Slacks Canyon (XSC) and Work Ranch (WKR), an along-strike distance of 31.2 km. 70% confidence intervals suggest that 15.8 to 27.0% of creep events observed at XSC are observed at WKR, and 10.2 to 19.6% of WKR events are observed at XSC (Figure 12d). These potentially long events are also observed at some of the creepmeters between them but not at all of the intermediate creepmeters. For instance, in Figure 12c, we have not plotted slip at XMD, XVA, and XTA because they displayed no creep event. Further, the percentage of XSC events observed at XMM and XPK are lower than the percentage of XSC events observed at WKR (Figure 12d).

We note, however, that much of the WKR-XSC correlation could be due to rainfall. If we remove events preceded by a 7-day interval with rainfall, 0.0 to 15.5% of XSC events are observed at WKR, and 0.0 to 13.0% of WKR events observed at XSC. Those percentages imply a 15% chance that the closely timed events result from hydrological forcing. If events with rainfall in the 14 days prior are removed, there are no closely timed events at XSC and WKR. Further, both XSC and WKR show a strong seasonal signal (Roeloffs, 2001); all of the closely timed creep events between these stations occur between December and March, showing a strong seasonal signal for these long events . Given both XSC and WKR prefer to slip in wet conditions (Figure S22), one might expect that these potential long events may instead be small local events that occurred at similar times due to atmospheric perturbations and rainfall.

5.5 Multi-strand Ruptures?

The coincidence of creep events on creepmeters separated by 8 km or perhaps even 30 km suggests that widely separated fault locations can communicate with each other on 24-hour timescales. However, the last set of closely timed creep events we examine suggest that creep event slip may spread not just over 8-km distances but also over multiple strands of the San Andreas Fault.

The two instrumented strands of interest are at the southern end of the creeping section, from Varian (XVA) to Carr Ranch (CRR). The main San Andreas Fault has creepmeters installed at Varian (XVA), Parkfield (XPK), Taylor Ranch (XTA), Work Ranch (WKR), and Carr Ranch (CRR). The southwest trace has two creepmeters, one at Roberson Southwest (XRSW) and another at Hearst Southwest (XHSW). We will focus on correlations with XHSW here because XRSW has too few events to allow robust statistics.

5.5.1 Hearst Southwest (XHSW) and the Main San Andreas Fault Creepmeters

Events at XHSW, on the southwest trace, display several creep events that are coincident with events on the main fault trace. 70% confidence intervals that suggest XHSW events are observed at many different creepmeters: Slacks Canyon (XSC) observes 2.7 to 13.3% of XHSW events, Middle Mountain (XMM) observed 23.7 to 45.2% of XHSW events , Varian (XVA) observes 0.2 to 12.0% of XHSW events, Parkfield (XPK) observes 11.9 to 31.7% of XHSW events; Work Ranch (WKR) observes 13.4 to 25.9% of XHSW events; and Carr Ranch (CRR) observes 0.3 to 11.4% of XHSW events (Figure 13a).

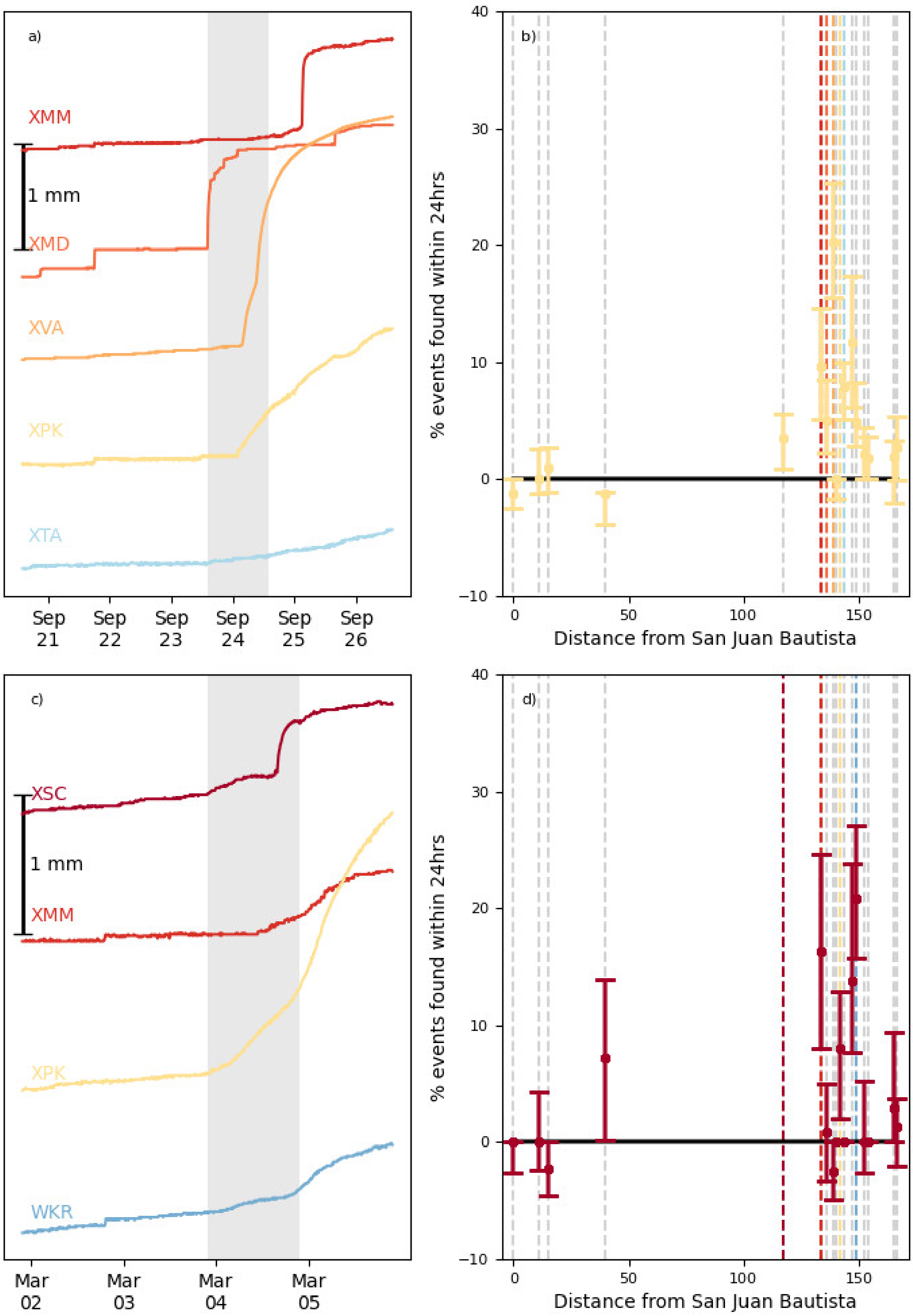

Figure 12. Potential large creep events from XSC - WKR section and percentage of events observed at other creepmeters for XPK and XSC. a) Creep event on the XMM - XTA section on 23rd - 25th September 2000. c) Creep event along the XSC - WKR section on 3rd - 4th March 1991. b) and d) indicate the percentage of XPK and XSC events found at other creepmeters, with 70% confidence intervals. Vertical colored lines in b) and d) mark the location of the creepmeters in a) and c).

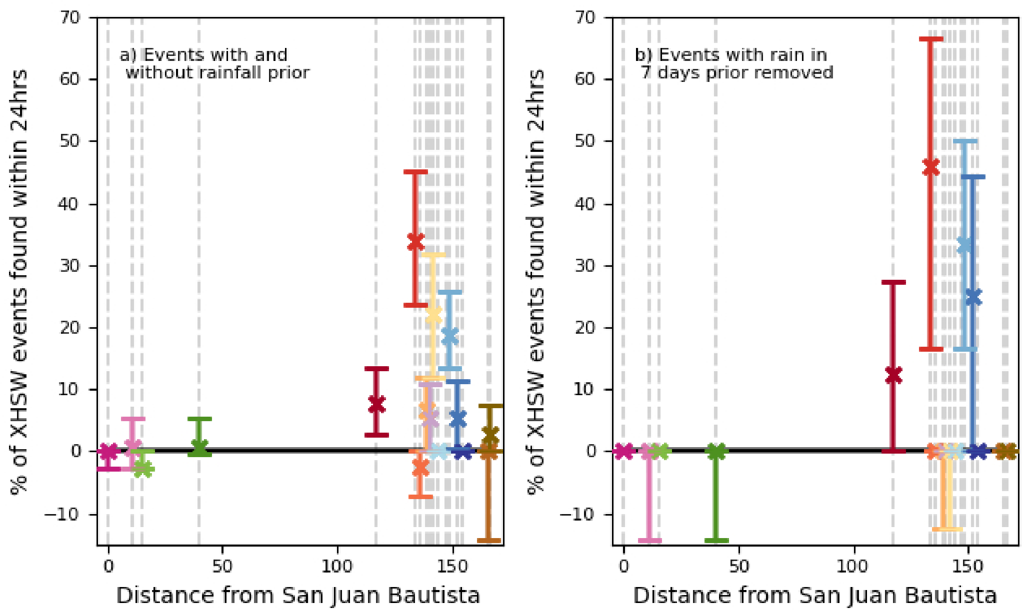

Figure 13. Scatter plots of the median percentage of creep events found at XHSW. In panel (a), all XHSW events are included. In panel (b), XHSW events with rainfall in the 7 days prior are removed.

Some of these percentages decrease to zero when we remove creep events preceded by rainfall. The correlations between XHSW and XVA and XPK could simply reflect a similar preference for slipping in wet conditions (Figure S24-S25). However, other correlations remain even when rainy intervals are removed (Figure 13b). XSC, XMM, WKR, and CRR all show evidence for coincident creep events, with XSC observing 0.0 to 27.3% of XHSW events, XMM observing 16.7 to 66.7% of XHSW events, WKR observing 16.7 to 50.0% of XHSW events, and CRR observing 0.0 to 44.4% of XHSW events. Both the XHSW at XSC and XHSW at CRR percentages intersect 0%, suggesting that their relationship may be arising by chance, despite not being driven by rainfall. XMM and WKR still observe a percentage of creep events from XHSW that is significant. WKR and XHSW are 2.12 km apart and are the closest creepmeters from each strand to one another. Their relationship remains even after rainfall effects are considered, implies that there might be an interaction between the two strands of the San Andreas Fault in this region, which appear to connect at >6 km depth (Waldhauser & Schaff, 2008; Center, 2014).

6 Short-term Rainfall Influence on Creep Events

The main goal of this study was to catalog creep events to identify creep event behaviors described in Section 5—to determine if creep events routinely rupture several or tens of km along strike. To do so, we examined the percentage of closely timed events at various pairs of creepmeters.

We compared our percentages with those expected for randomly timed creep events in a way that preserved any seasonality in the creep event records. However, creepmeters and creep events can also be triggered by hydrological variations on shorter timescales (Roeloffs, 2001; Schulz, 1989). To assess whether the closely timed events observed at relatively distant creepmeters come from long along-strike ruptures or from a coincident response to rainfall, we redid our analysis after excluding creep events preceded by 3-, 7-, or 14-day intervals that included rainfall. We summarized the implications of those results for inferring creep event sizes in Section 5. However, a more thorough investigation of rainfall responses could teach us more about creep event behaviors. We do not attempt a thorough investigation here, but we briefly discuss why excluding rainfall could leave inter-creepmeter correlations in creep event timing decreased, unchanged, or increased.

6.1 Percentage of Correlated Events Decreases

For some creepmeters pairings, the percentage of closely timed creep decreases when we remove events preceded by rainy intervals. Figure 14a shows this effect for the XSC and WKR pair. Both creepmeters are seasonally modulated, with more events in the winter months (Roeloffs, 2001). When we preserve this seasonality but randomize times on shorter timescales (see Section 4.2), we can assess the local creep events' preference for rainfall, and we find that both creepmeters display more events in wet conditions (Figure S22).

When two creepmeters have a common response to rainfall, we expect that some closely timed events coincide because they both respond to rainfall, not because a larger creep event connects the creepmeters. By removing times preceded by rainfall, we remove the largest-amplitude forcing and expect a reduction in the correlated response. For the XSC-WKR pair, the reduction is significant. When we remove events with rainfall in the 7 days prior, the lower bound of the 70% confidence interval is 0. There is a 15% chance that none of the closely timed creep events reflect spatially expansive creep events. All of them could be coincidental responses to hydrological perturbations.

6.2 Percentage of Correlated Events Remains Unchanged

Intriguingly, however, we most commonly find that the percentage of closely timed events remains unchanged when we remove rainy intervals. The median percentage for the XMM-XMD pair, for instance, remains around 14.5%, increasing marginally to 15.9%, as we remove intervals with rainfall(Figure 14b). The lack of change in closely spaced events implies that the creep events respond minimally to short-timescale variations in rainfall or that the responses are uncorrelated at the two creepmeters. While it seems somewhat surprising that short-timescale rainfall responses are commonly uncorrelated between creepmeter locations, it makes many interpretations simple. Since the closely timed creep events are unaffected by rainfall, the correlations must be driven by something else, most likely slip at depth.

6.3 Percentage of Correlated Events Increases

However, for one creepmeter pair (XHR-CWN), we find a more dramatic *increase* in the percentage of closely timed events, from 25 to 40%, when we remove events preceded by a 14-day interval that includes rainfall(Figure 14c). Such a significant change may suggest that small, single-creepmeter creep events respond differently to rainfall than larger, multi-creepmeter events that rupture at depth. Perhaps there are small, shallow events at XHR and CWN that are often triggered by rain. We may remove these small events when we remove rainy intervals, retaining only deeper creep events that span both creepmeters.

7 Discussion

We have identified over 2000 long and short creep events along the San Andreas Fault using cross-correlation, slip thresholding, and manual inspection. Using this catalog, we identified a variety of creep event behaviors. Some creep events are observed only at individual creepmeters, while others appear to rupture to neighboring creepmeters. We have also determined that most of these longer multi-creepmeter events are not rainfall induced; evidence for 2, 5 and, 10-km long creep events remains robust when rainfall influences are excluded.

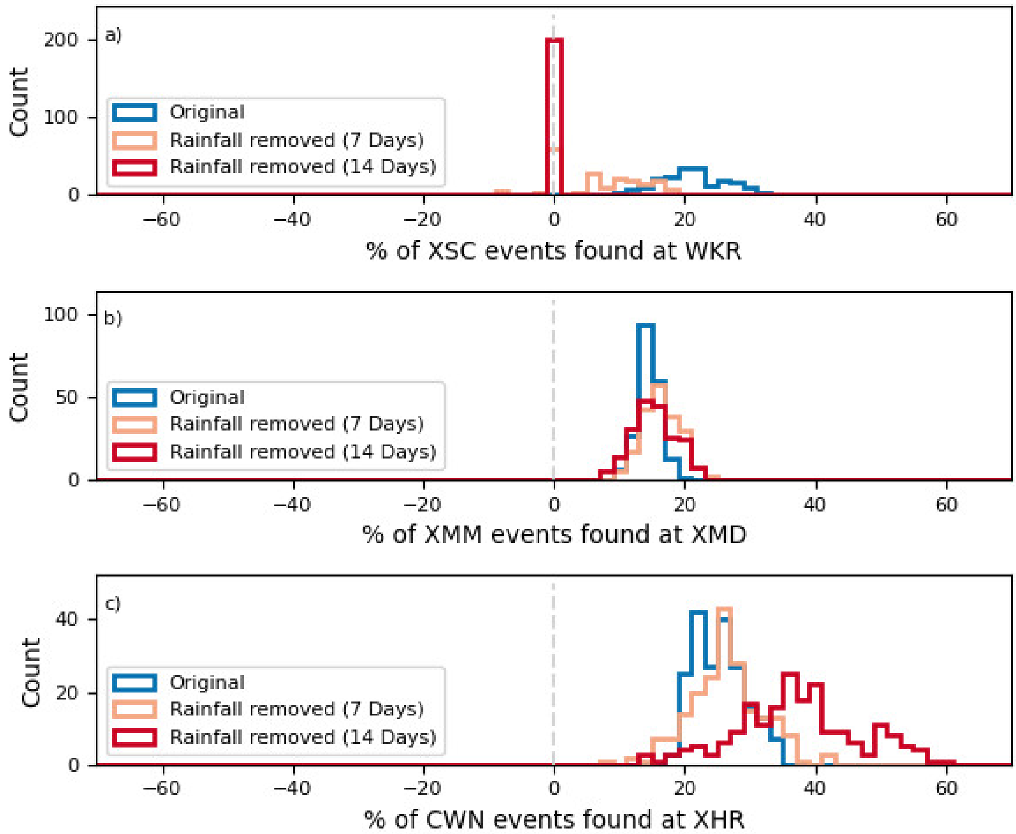

Figure 14. Percentage of creep events observed at pairs of creepmeters accounting for rainfall. a) Percentage of XSC events observed at WKR. b) Percentage of XMM events observed at XMD. c) Percentage of CWN events observed at XHR. In a), b) and c) the original percentages are in blue, and the percentage of events after accounting for rainfall in the previous 7- or 14-days are orange and red, respectively.

7.1 What Drives Creep Events?

Since the discovery of creep events in the 1960s, there have been many different models proposed to drive creep events. Here we discuss different models for the driving of creep events and discuss their plausibility in the light of our observed rupture lengths.

For instance, in one model of creep events, the San Andreas Fault could have a slip rate-strengthening rheology near the surface. Creep events could arise simply with this nominally stable rheology simply because rainfall and atmospheric pressure perturbations "kick" the fault, and the fault's resistance to slip is low at near-surface, low-stress conditions (Kanu & Johnson, 2011; Helmstetter & Shaw, 2009; Perfettini & Ampuero, 2008). However, it is hard to explain how creep events commonly extend 5 km along strike if they result from small, near-surface stress perturbations.

We also note that some creep events' timings appear indifferent to rainfall, so rain does not provide an obvious driving perturbation. On the other hand, groundwater-driven perturbations could occur later than rainfall, and the fault could accelerate with a time lag, so a lack of timing with rainfall does not exclude this perturbed rate-strengthening model.

Nevertheless, it would seem more plausible that creep events are driven by frictional weakening of the fault, which drives accelerating albeit aseismic slip. There could be patches or layers of slip-rate weakening material that have a particular size: which are large enough to accelerate into creep events but which are too small to grow into a seismic rupture (Liu & Rice, 2005, 2007; Rubin, 2008; Wei et al., 2013). Such layered rheologies could help explain the kinematics and size distribution of creep events (Bilham & Behr, 1992; Gladwin et al., 1994; Bilham et al., 2016). However, fixed material-dependent layers may not explain all the observed kinematics of creep events. For instance, the boundary between an upper stably slipping and a deeper more unstable layer was proposed to deepen following the 1989 Loma Prieta earthquake (Behr et al., 1997).

The biggest problem with a rate-weakening patch model is that it may be implausible to get patches of rate-weakening material have just the right size to allow creep events but not earthquakes (Rubin, 2008). But one could imagine that there are many layers or patches of rate-weakening material scattered along a mostly rate-strengthening fault. Perhaps just some of them host creep events. Individual fault patches could give rise to single creepmeter events (Section 5.1). For multi-creepmeter events, many fault patches may have to rupture.

Such patch sizes must still be tuned. They must be small enough and far enough apart to prevent dynamic rupture but close enough together to allow aseismic rupture propagation (Ando et al., 2010; Skarbek et al., 2012; Luo & Ampuero, 2018; Yabe & Ide, 2017). It remains unclear whether such tuning is too precise to be plausible, but we do know that faults are rough and heterogeneous (e.g., Candela et al., 2012; Brodsky et al., 2016; Candela & Brodsky, 2016; Thom et al., 2017). That heterogeneity is increasingly incorporated into frictional models (e.g., Fang & Dunham, 2013; Dieterich & Smith, 2009; Romanet et al., 2018)

Given the apparent tuning issues involved in heterogeneity, one might prefer to explain creep events using a different fault zone process: something that promotes initial acceleration but eventually limits slip speeds at a local scale. At the shallow depths of creep events, shear-induced fault dilatancy is an plausible candidate (Segall & Rice, 1995; Segall et al., 2010; Iverson, 2005). Previous studies have shown that shear-induced dilatancy may limit slip rates at shallow depths, preventing runaway slip in landslides (e.g., Iverson, 2005). In the dilatancy model, the fault zone dilates as it starts to accelerate. The dilation causes a reduced pore pressure, which sucks the fault shut and discourages further slip. Some limited support for dilatancy comes from an indication that pore pressure changes during creep events; the well water level rises or fall during creep events between Middle Mountain (XMM) and Middle Ridge (XMD) (Roeloffs et al., 1989; Rudnicki et al., 1993).

7.2 Propagation at Depth

Although we cannot be conclusive about the physical mechanism that drives creep events, we can describe some of the kinematics of slip. Most intriguingly, we sometimes find that creep events skip creepmeters as they propagate. The lack of slip at intermediate locations could indicate that creep events propagate largely in a deeper layer and do not always reach the surface (Evans et al., 1981; Bilham & Behr, 1992). Alternatively, the skipped surface locations could indicate that the near-surface fault conditions temporarily discourage abrupt slip, perhaps because the stress is low. For instance, the stress could be low, or a locally stable patch could prevent rupture as the creep event propagates past (e.g., Luo & Ampuero, 2018).

7.3 Moment Accommodated by Creep Events?

Though we cannot directly constrain the depth of slip using creepmeter data, the skipped creepmeters noted in Section 7.2, along with the relatively large along-strike extents of some events, suggest that creep events could extend to significant depth—to depths of kilometers to rather than 100s of meters. And if creep events extend to significant depth, they could have significant moment. Groups of creep events might modulate the moment budget of the San Andreas Fault on decadal or centennial timescales.

Such modulation is interesting to consider because geodetic and repeating earthquake observations have been used to observe variations in the faults' creep rate, with some suggesting this variation occurs on decadal timescales. (Nadeau & McEvilly, 2004; Khoshmanesh & Shirzaei, 2018a, 2018b; Khoshmanesh et al., 2015; Templeton et al., 2009; Sammis et al., 2016). Further, large creep events have been reported on the San Andreas Fault and elsewhere (Linde et al., 1996; Roeloffs, 2001; Martínez-Garzón et al., 2019). And a few creepmeters display differently shaped, longer creep events events. While most of the creepmeters we examined accumulate 50 to 75% of their slip in the small creep events examined here creepmeters XSC and XTA creepmeters accumulate only 5 to 10% of their slip in small events. Much of the remaining slip accumulates in longer surges of slip, which have an indistinct onset but last weeks to months.

Current geodetic estimates suggest the San Andreas Fault's central creeping section is currently slipping slightly more slowly than its long term rate. The low slip rate could lead to a M_w 5.2 – 7.2 earthquake every 150 (Maurer & Johnson, 2014; Ryder & Bürgmann, 2008; Michel et al., 2018). Alternatively, if creep events play an important role in reducing the creeping region's slip deficit, the low slip rate could lead to a cluster of 30 $M_W 4$ creep events rather than a $M_W 5$ earthquake. To give that moment context, $M_W 4$ creep event could be a 4-km long, 4-km deep event with 2 mm of slip. A 4-km long, 1-km deep event with 2 mm would have moment equivalent to a $M_W 3.6$ earthquake.

We note, of course, that estimating the possible moments of creep events does not tell us whether clusters of tens or hundreds of creep events can occur. To assess the plausible variability of creep events, we would need to better understand the driving physics (Section 7.1). That physics may eventually help us assess whether creeping regions can also rupture in earthquakes and pose a seismic hazard (e.g., Harris (2017)). Many creeping faults appear to be barriers to seismic propagation (e.g., Ryder and Bürgmann (2008); Thomas et al. (2014); Titus (2006); Nocquet et al. (2017)), but laboratory-based faults often display strong weakening at m/s slip rates, and that dynamic weakening could allow a normally creeping region to rupture in an earthquake (Noda & Lapusta, 2013).

8 Conclusion

In this study, we have identified and correlated 2120 creep events recorded on creepmeters along the creeping section of the San Andreas Fault between 1985 and 2020. Some of these creep event detections occur simultaneously at two or more creepmeters; we identify 306 potential events that could rupture multiple creepmeters. Our analysis allows us to identify five groups of creep events: (1) isolated events, (2) small (<2km) events, (3) medium-sized (3-6 km) events, (4) large events (>10 km), and (5) events that rupture multiple strands. The vast majority of these events are not affected by rainfall. Correlations between creepmeters persist when rainfall influences are excluded. The length of the creep events observed helps us assess the plausibility of different driving models for creep events; local frictional weakening, perhaps with a complex rheology, seems most possible. The creep event lengths, when coupled with the kinematics of slip at various creepmeters, also suggest that creep events rupture both at the surface and at depth. Determining the depth of this slip, and thus of creep events, is an essential next step in understanding the role of creep events in the overall slip dynamics of the creeping section.

Acknowledgments

This work was funded by the Natural Environment Research Council grant number NE/S007474/1. Creep data are provided by the United States Geological Survey and are available at https://earthquake.usgs.gov/monitoring/deformation/data/download.php. The plotted fault traces are taken from the Quaternary fault and fold database for the United States, provided by the USGS and the California Geological Survey, and accessed from the USGS website https://www.usgs.gov/natural-hazards/earthquake-hazards/faults. Rainfall data are provided by the National Oceanic and Atmospheric Administration and are available at https://www.ncdc.noaa.gov/cdo-web/datasets. We thank Hui Huang for providing insight into fault structure at depth, by examining earthquake locations provided through the Northern California Earthquake Data Center (NCEDC), doi:10.7932/NCEDC.

References

Ambraseys, N. (1970). Some characteristic features of the Anatolian fault zone. *Tectonophysics*, *9*(2-3), 143–165. doi: 10.1016/0040-1951(70)90014-4

Ando, R., Nakata, R., & Hori, T. (2010). A slip pulse model with fault heterogeneity for low-frequency earthquakes and tremor along plate interfaces: Slip pulse model for tremor. *Geophys. Res. Lett.*, *37*(10). doi: 10.1029/2010GL043056

Behr, J., Bilham, R., Bodin, P., Breckenridge, K., & Sylvester, A. G. (1997). Increased surface creep rates on the San Andreas Fault southeast of the Loma Prieta Main Shock. In P. A. Reasenberg (Ed.), *The Loma Prieta, California, Earthquake of October 17, 1989 - Aftershocks and Postseismic Effects* (pp. 179–192). U.S. Government Printing Office.

Bilham, R., & Behr, J. (1992). A two-layer model for aseismic slip on the superstition hills fault, california. *Bulletin of the Seismological Society of America*, *82*(3), 1223–1235.

Bilham, R., & Castillo, B. (2020). The July 2019 Ridgecrest, California, Earthquake Sequence Recorded by Creepmeters: Negligible Epicentral Afterslip and Prolonged Triggered Slip at Teleseismic Distances. *Seismological Research Letters*, *91*(2A), 707–720. doi: 10.1785/0220190293

Bilham, R., Ozener, H., Mencin, D., Dogru, A., Ergintav, S., Cakir, Z., ... Mattioli, G. (2016). Surface creep on the North Anatolian Fault at Ismetpasa, Turkey, 1944–2016. *J. Geophys. Res. Solid Earth*, *121*, 7409–7431.

Brodsky, E. E., Kirkpatrick, J. D., & Candela, T. (2016). Constraints from fault roughness on the scale-dependent strength of rocks. *Geology*, *44*(1), 19–22. doi: 10.1130/G37206.1

Candela, T., & Brodsky, E. E. (2016). The minimum scale of grooving on faults. *Geology*, *44*(8), 603–606. doi: 10.1130/G37934.1

Candela, T., Renard, F., Klinger, Y., Mair, K., Schmittbuhl, J., & Brodsky, E. E. (2012). Roughness of fault surfaces over nine decades of length scales. *J. Geophys. Res.*, *117*(B8). doi: 10.1029/2011JB009041

Center, N. C. E. D. (2014). *Northern California Earthquake Data Center.* UC Berkeley Seismological Laboratory. Retrieved from `http://ncedc.org/ncedc_doi_metadata.html` (Type: dataset) doi: 10.7932/NCEDC

Dieterich, J. H., & Smith, D. E. (2009). Nonplanar Faults: Mechanics of Slip and Off-fault Damage. *Pure appl. geophys.*, *166*(10-11), 1799–1815. doi: 10.1007/s00024-009-0517-y

Duquesnoy, T., Barrier, E., Kasser, M., Aurelio, M., Gaulon, R., Punongbayan, R. S., & Rangin, C. (1994). Detection of creep along the Philippine Fault: First results of geodetic measurements on Leyte Island, central Philippine. *Geophysical Research Letters*, *21*(11), 975–978.

Evans, K. F., Burford, R. O., & King, G. C. P. (1981). Propagating episodic creep and the aseismic slip behavior of the Calaveras Fault north of Hollister, California. *J. Geophys. Res.*, *86*(B5), 3721. doi: 10.1029/JB086iB05p03721

Fang, Z., & Dunham, E. M. (2013). Additional shear resistance from fault roughness and stress levels on geometrically complex faults. *Journal of Geophysical Research: Solid Earth*, *118*(7), 3642–3654. doi: 10.1002/jgrb.50262

Fattahi, H., & Amelung, F. (2016). InSAR observations of strain accumulation and fault creep along the Chaman Fault system, Pakistan and Afghanistan: Strain Accumulation at Chaman Fault. *Geophys. Res. Lett.*, *43*(16), 8399–8406. doi: 10.1002/2016GL070121

Gladwin, M. T., Gwyther, R. L., Hart, R. H. G., & Breckenridge, K. S. (1994). Measurements of the strain field associated with episodic creep events on the San Andreas Fault at San Juan Bautista, California. *J. Geophys. Res.*, *99*(B3), 4559–4565. doi: 10.1029/93JB02877

Goulty, N. R., & Gilman, R. (1978). Repeated creep events on the San Andreas Fault near Parkfield, California, Recorded by a strainmeter array. *Journal of Geophysical Research*, *83*(B11).

Harris, R. A. (2017). Large earthquakes and creeping faults. *Reviews of Geophysics*, *55*(1), 169–198. doi: https://doi.org/10.1002/2016RG000539

Helmstetter, A., & Shaw, B. E. (2009). Afterslip and aftershocks in the rate-and-state friction law. *Journal of Geophysical Research: Solid Earth*, *114*(B1). doi: 10.1029/2007JB005077

Iverson, R. M. (2005). Regulation of landslide motion by dilatancy and pore pressure feedback. *Journal of Geophysical Research: Earth Surface*, *110*(F2). Retrieved from `https://agupubs.onlinelibrary.wiley.com/doi/abs/10.1029/2004JF000268` doi: 10.1029/2004JF000268

Jolivet, R., Lasserre, C., Doin, M.-P., Peltzer, G., Avouac, J.-P., Sun, J., & Dailu, R. (2013). Spatio-temporal evolution of aseismic slip along the Haiyuan fault, China: Implications for fault frictional properties. *Earth and Planetary Science Letters*, *377-378*, 23–33. doi: 10.1016/j.epsl.2013.07.020

Jolivet, R., Simons, M., Agram, P. S., Duputel, Z., & Shen, Z.-K. (2015). Aseismic slip and seismogenic coupling along the central San Andreas Fault. *Geophys. Res. Lett.*, *42*(2), 297–306. doi: 10.1002/2014GL062222

Kanu, C., & Johnson, K. (2011). Arrest and recovery of frictional creep on the southern Hayward fault triggered by the 1989 Loma Prieta, California, earthquake and implications for future earthquakes. *J. Geophys. Res.*, *116*(B4), B04403. doi: 10.1029/2010JB007927

Khoshmanesh, M., & Shirzaei, M. (2018a). Episodic creep events on the San Andreas Fault caused by pore pressure variations. *Nature Geoscience*, *11*(8), 610–614. doi: 10.1038/s41561-018-0160-2

Khoshmanesh, M., & Shirzaei, M. (2018b). Multiscale Dynamics of Aseismic Slip on Central San Andreas Fault. *Geophys. Res. Lett.*, *45*(5), 2274–2282. doi: 10.1002/

2018GL077017

Khoshmanesh, M., Shirzaei, M., & Nadeau, R. M. (2015). Time-dependent model of aseismic slip on the central San Andreas Fault from InSAR time series and repeating earthquakes. *J. Geophys. Res. Solid Earth*, *120*(9), 6658–6679. doi: 10.1002/2015JB012039

King, C.-Y., Nason, R. D., & Tocher, D. (1973). Kinematics of Fault Creep. *Philosophical Transactions of the Royal Society of London. Series A, Mathematical and Physical Sciences*, *274*(1239), 355–360. (Publisher: The Royal Society)

Langbein, J., Borcherdt, R., Dreger, D., Fletcher, J., Hardebeck, J. L., Hellweg, M., ... Treiman, J. A. (2005). Preliminary Report on the 28 September 2004, M 6.0 Parkfield, California Earthquake. *Seismological Research Letters*, *76*(1), 10–26. doi: 10.1785/gssrl.76.1.10

Langbein, J., & Johnson, H. (1997). Correlated errors in geodetic time series: Implications for time-dependent deformation. *Journal of Geophysical Research: Solid Earth*, *102*(B1), 591–603. Retrieved from `https://agupubs.onlinelibrary.wiley.com/doi/abs/10.1029/96JB02945` doi: https://doi.org/10.1029/96JB02945

Langbein, J., Quilty, E., & Breckenridge, K. (1993). Sensitivity of crustal deformation instruments to changes in secular rate. *Geophys. Res. Lett.*, *20*(2), 85–88. doi: 10.1029/92GL02718

Lee, J.-C., Angelier, J., Chu, H.-T., Hu, J.-C., & Jeng, F.-S. (2005). Monitoring active fault creep as a tool in seismic hazard mitigation. Insights from creepmeter study at Chihshang, Taiwan. *Comptes Rendus Geoscience*, *337*, 1200-1207. doi: 10.1016/j.crte.2005.04.018

Leeman, J. R., Marone, C., & Saffer, D. M. (2018). Frictional Mechanics of Slow Earthquakes. *Journal of Geophysical Research: Solid Earth*, *123*(9), 7931–7949. doi: 10.1029/2018JB015768

Lienkaemper, J. J. (2006). Surface Slip Associated with the 2004 Parkfield, California, Earthquake Measured on Alinement Arrays. *Bulletin of the Seismological Society of America*, *96*(4B), S239–S249. doi: 10.1785/0120050806

Lienkaemper, J. J., McFarland, F. S., Simpson, R. W., Bilham, R. G., Ponce, D. A., Boatwright, J. J., & Caskey, S. J. (2012). Long-Term Creep Rates on the Hayward Fault: Evidence for Controls on the Size and Frequency of Large Earthquakes. *Bulletin of the Seismological Society of America*, *102*(1), 31–41. doi: 10.1785/0120110033

Linde, A. T., Gladwin, M. T., Johnston, M. J. S., Gwyther, R. L., & Bilham, R. G. (1996). A slow earthquake sequence on the San Andreas fault. *Nature*, *383*(6595), 65–68. doi: 10.1038/383065a0

Lisowski, M., & Prescott, W. H. (1981). Short-range distance measurements along the San Andreas fault system in central California, 1975 to 1979. *Bulletin of the Seismological Society of America*, *71*(5), 1607–1624.

Liu, Y., & Rice, J. R. (2005). Aseismic slip transients emerge spontaneously in three-dimensional rate and state modeling of subduction earthquake sequences. *Journal of Geophysical Research: Solid Earth*, *110*(B8). doi: https://doi.org/10.1029/2004JB003424

Liu, Y., & Rice, J. R. (2007). Spontaneous and triggered aseismic deformation transients in a subduction fault model. *J. Geophys. Res.*, *112*(B9), B09404. doi: 10.1029/2007JB004930

Luo, Y., & Ampuero, J.-P. (2018, May). Stability of faults with heterogeneous friction properties and effective normal stress. *Tectonophysics*, *733*, 257–272. doi: 10.1016/j.tecto.2017.11.006

Martínez-Garzón, P., Bohnhoff, M., Mencin, D., Kwiatek, G., Dresen, G., Hodgkinson, K., ... Kartal, R. F. (2019). Slow strain release along the eastern Marmara region offshore Istanbul in conjunction with enhanced local seismic moment release. *Earth and Planetary Science Letters*, *510*, 209–218. doi: 10.1016/j.epsl.2019.01.001

Maurer, J., & Johnson, K. (2014). Fault coupling and potential for earthquakes on the creeping section of the central San Andreas Fault: Fault coupling on the creeping SAF. *J. Geophys. Res. Solid Earth*, *119*(5), 4414–4428. doi: 10.1002/2013JB010741

Michel, S., Avouac, J.-P., Jolivet, R., & Wang, L. (2018). Seismic and Aseismic Moment Budget and Implication for the Seismic Potential of the Parkfield Segment of the San Andreas FaultSeismic and Aseismic Moment Budget and Implication for the Seismic Potential of the Parkfield Segment of the SAF. *Bulletin of the Seismological Society of America*, *108*(1), 19–38. doi: 10.1785/0120160290

Nadeau, R. M., & McEvilly, T. V. (2004). Periodic Pulsing of Characteristic Microearthquakes on the San Andreas Fault. *Science*, *303*(5655), 220–222. doi: 10.1126/science.1090353

Nocquet, J.-M., Jarrin, P., Vallée, M., Mothes, P. A., Grandin, R., Rolandone, F., ... Charvis, P. (2017). Supercycle at the Ecuadorian subduction zone revealed after the 2016 Pedernales earthquake. *Nature Geosci*, *10*(2), 145–149. doi: 10.1038/ngeo2864

Noda, H., & Lapusta, N. (2013). Stable creeping fault segments can become destructive as a result of dynamic weakening. *Nature*, *493*(7433), 518–521. doi: 10.1038/nature11703

Perfettini, H., & Ampuero, J.-P. (2008, September). Dynamics of a velocity strengthening fault region: Implications for slow earthquakes and postseismic slip. *J. Geophys. Res.*, *113*(B9), B09411. doi: 10.1029/2007JB005398

Roeloffs, E. A. (2001). Creep rate changes at Parkfield, California 1966-1999: Seasonal, precipitation induced, and tectonic. *J. Geophys. Res.*, *106*(B8), 16525–16547. doi: 10.1029/2001JB000352

Roeloffs, E. A., Burford, S. S., Riley, F. S., & Records, A. W. (1989). Hydrologic effects on water level changes associated with episodic fault creep near Parkfield, California. *J. Geophys. Res. Solid Earth*, *94*(B9), 12,387–12,402. doi: 10.1029/JB094iB09p12387

Romanet, P., Bhat, H. S., Jolivet, R., & Madariaga, R. (2018). Fast and Slow Slip Events Emerge Due to Fault Geometrical Complexity. *Geophysical Research Letters*, *45*(10), 4809–4819. doi: 10.1029/2018GL077579

Rousset, B., Fu, Y., Bartlow, N., & Bürgmann, R. (2019). Weeks-Long and Years-Long Slow Slip and Tectonic Tremor Episodes on the South Central Alaska Megathrust. *J. Geophys. Res. Solid Earth*, *124*(12), 13392–13403. doi: 10.1029/2019JB018724

Rousset, B., Jolivet, R., Simons, M., Lasserre, C., Riel, B., Milillo, P., ... Renard, F. (2016). An aseismic slip transient on the North Anatolian Fault. *Geophysical Research Letters*, *43*(7), 3254–3262. doi: https://doi.org/10.1002/2016GL068250

Rubin, A. M. (2008). Episodic slow slip events and rate-and-state friction. *J. Geophys. Res.*, *113*(B11), B11414. doi: 10.1029/2008JB005642

Rudnicki, J. W., Yin, J., & Roeloffs, E. A. (1993). Analysis of water level changes induced by fault creep at Parkfield, California. *J. Geophys. Res.*, *98*(B5), 8143–8152. doi: 10.1029/93JB00354

Ryder, I., & Bürgmann, R. (2008). Spatial variations in slip deficit on the central San Andreas Fault from InSAR. *Geophysical Journal International*, *175*(3), 837–852. doi: 10.1111/j.1365-246X.2008.03938.x

Sammis, C. G., Smith, S. W., Nadeau, R. M., & Lippoldt, R. (2016). Relating Transient Seismicity to Episodes of Deep Creep at Parkfield, California. *Bulletin of the Seismological Society of America*, *106*(4), 1887–1899. doi: 10.1785/0120150224

Schulz, S. (1989). *Catalog of creepmeter measurements in california from 1966 through 1988* (U.S. Geol. Surv. Open File Rep No. 89-650).

Segall, P., & Rice, J. R. (1995). Dilatancy, compaction, and slip instability of a fluid-infiltrated fault. *J. Geophys. Res.*, *100*(B11), 22155–22171. doi: 10.1029/95JB02403

Segall, P., Rubin, A. M., Bradley, A. M., & Rice, J. R. (2010). Dilatant strengthening as a mechanism for slow slip events. *J. Geophys. Res.*, *115*(B12), B12305. doi: 10.1029/2010JB007449

Shibazaki, B., & Iio, Y. (2003). On the physical mechanism of silent slip events along the deeper part of the seismogenic zone. *Geophysical Research Letters*, *30*(9). doi: 10.1029/2003GL017047

Skarbek, R. M., Rempel, A. W., & Schmidt, D. A. (2012). Geologic heterogeneity can produce aseismic slip transients. *Geophys. Res. Lett.*, *39*(21). doi: 10.1029/2012GL053762

Steinbrugge, K. V., Zacher, E. G., Tocher, D., Whitten, C. A., & Claire, C. N. (1960). Creep on the San Andreas fault. *Bulletin of the Seismological Society of America*, *50*(3), 389–415.

Templeton, D. C., Nadeau, R. M., & Bürgmann, R. (2009). Distribution of postseismic slip on the Calaveras fault, California, following the 1984 M6.2 Morgan Hill earthquake. *Earth and Planetary Science Letters*, *277*(1), 1–8. doi: 10.1016/j.epsl.2008.09.024

Thom, C. A., Brodsky, E. E., Carpick, R. W., Pharr, G. M., Oliver, W. C., & Goldsby, D. L. (2017). Nanoscale Roughness of Natural Fault Surfaces Controlled by Scale-Dependent Yield Strength: Nanoscale Fault Roughness and Strength. *Geophys. Res. Lett.*, *44*(18), 9299–9307. doi: 10.1002/2017GL074663

Thomas, M. Y., Avouac, J.-P., Champenois, J., Lee, J.-C., & Kuo, L.-C. (2014). Spatiotemporal evolution of seismic and aseismic slip on the Longitudinal Valley Fault, Taiwan. *J. Geophys. Res. Solid Earth*, *119*(6), 5114–5139. doi: 10.1002/2013JB010603

Titus, S. J. (2006). Thirty-Five-Year Creep Rates for the Creeping Segment of the San Andreas Fault and the Effects of the 2004 Parkfield Earthquake: Constraints from Alignment Arrays, Continuous Global Positioning System, and Creepmeters. *Bulletin of the Seismological Society of America*, *96*(4B), S250–S268. doi: 10.1785/0120050811

Titus, S. J., Dyson, M., DeMets, C., Tikoff, B., Rolandone, F., & Burgmann, R. (2011). Geologic versus geodetic deformation adjacent to the San Andreas fault, central California. *Geological Society of America Bulletin*, *123*(5-6), 794–820. doi: 10.1130/B30150.1

Toppozada, T. R., Branum, D. M., Reichle, M. S., & Hallstrom, C. L. (2002). San Andreas Fault Zone, California: M $\geq$ 5.5 Earthquake History. *Bulletin of the Seismological Society of America*, *92*(7), 2555–2601. doi: 10.1785/0120000614

Waldhauser, F., & Schaff, D. P. (2008). Large-scale relocation of two decades of Northern California seismicity using cross-correlation and double-difference methods. *J. Geophys. Res.*, *113*(B8). Retrieved from `https://onlinelibrary.wiley.com/doi/10.1029/2007JB005479` doi: 10.1029/2007JB005479

Wei, M., Kaneko, Y., Liu, Y., & McGuire, J. J. (2013). Episodic fault creep events in California controlled by shallow frictional heterogeneity. *Nature Geosci*, *6*(7), 566–570. doi: 10.1038/ngeo1835

Yabe, S., & Ide, S. (2017). Slip-behavior transitions of a heterogeneous linear fault. *Journal of Geophysical Research: Solid Earth*, *122*(1), 387–410. Retrieved from `https://agupubs.onlinelibrary.wiley.com/doi/abs/10.1002/2016JB013132` doi: 10.1002/2016JB013132